Summary of Neutrino Interaction Rates for VLBNO Experiments

Mary Bishai[1], Brett Viren[1]

[1] *Brookhaven National Laboratory, P.O. Box 5000, Upton, NY 11950, USA*

(Dated: January 26, 2007)

Abstract

Summary of Monte Carlo estimates of neutrino interaction rates for various NuMI off-axis energy and beam configurations and FNAL-DUSEL Wide-Band Low-Energy (WBLE) beams.

Distance off-axis	ν_μ CC	ν_μ CC osc	ν_e CC beam	ν_e QE beam	NC-1π^0	$\nu_\mu \to \nu_e$ CC	$\nu_\mu \to \nu_e$ QE
NuMI LE tune at 700 km							
0 km	400.2	267.6	4.55	0.444	21.2	3.66	0.676
40 km	4.81	2.66	0.190	0.047	0.525	0.071	0.038
NuMI LE tune at 810 km							
0 km	299.0	187.4	3.40	0.332	15.8	3.10	0.551
6 km	198.6	107.0	2.59	0.275	11.9	2.53	0.506
12 km	84.4	31.9	1.57	0.193	6.79	1.41	0.367
30 km	11.6	8.38	0.353	0.070	1.32	0.107	0.046
40 km	5.38	2.91	0.195	0.045	0.596	0.084	0.045
NuMI ME tune at 810 km							
0 km	949.1	781.1	7.14	0.485	30.6	4.71	0.527
6 km	304.9	191.4	3.83	0.313	14.9	3.19	0.491
12 km	80.5	32.0	1.81	0.174	5.74	1.33	0.330
30 km	8.59	5.52	0.321	0.051	0.81	0.094	0.038
40 km	4.14	2.40	0.168	0.032	0.427	0.054	0.022

TABLE I: Signal and background interaction rates for various NuMI beam configurations, baselines and off-axis distances. Rates are given per MW.10^7s.kT. The rates are integrated over the range 0-20 GeV. For $\nu_\mu \to \nu_e$ oscillations a value of $\sin^2 2\theta_{13} = 0.04$ and $\Delta m^2_{31} = 2.5 \times 10^{-3}$ eV^2 is used. No detector model is used.

Distance off-axis	$\bar{\nu}_\mu$ CC	$\bar{\nu}_\mu$ CC osc	$\bar{\nu}_e$ CC beam	$\bar{\nu}_e$ QE beam	NC-1π^0	$\bar{\nu}_\mu \to \bar{\nu}_e$ CC	$\bar{\nu}_\mu \to \bar{\nu}_e$ QE
NuMI LE tune at 700 km							
0 km	157.6	102.3	1.69	0.306	19.3	1.25	0.306
40 km	1.64	0.905	0.063	0.021	0.544	0.024	0.016
NuMI LE tune at 810 km							
0 km	117.7	71.0	1.26	0.229	14.4	1.026	0.285
6 km	77.6	39.8	0.925	0.179	10.8	0.800	0.241
12 km	31.7	10.9	0.545	0.116	6.29	0.388	0.145
30 km	3.87	2.69	0.122	0.035	1.31	0.043	0.025
40 km	1.81	0.97	0.066	0.021	0.609	0.029	0.018
NuMI ME tune at 810 km							
0 km	350.6	285.1	2.53	0.349	23.6	1.59	0.316
6 km	112.8	69.0	1.28	0.208	11.9	1.011	0.259
12 km	27.7	9.83	0.601	0.105	4.76	0.348	0.125
30 km	2.66	1.67	0.109	0.027	0.70	0.027	0.014
40 km	1.27	0.73	0.057	0.016	0.376	0.015	0.008

TABLE II: Signal and background interaction rates for various NuMI anti-neutrino beam configurations, baselines and off-axis distances. Rates are given per MW.10^7s.kT. The rates are integrated over the range 0-20 GeV. For $\nu_\mu \to \nu_e$ oscillations a value of $\sin^2 2\theta_{13} = 0.04$ and $\Delta m^2_{31} = 2.5 \times 10^{-3}$ eV^2 is used. No detector model is used.

Degrees off-axis	ν_μ CC	ν_μ CC osc	ν_e CC beam	ν_e QE beam	NC-1π^0	$\nu_\mu \to \nu_e$ CC	$\nu_\mu \to \nu_e$ QE
WBLE 120 GeV at 1300 km with decay pipe 2m radius 380 m length							
0°	198.2	104.9	1.89	0.179	9.11	2.85	0.408
0.5°	89.9	37.9	1.22	0.140	5.62	1.62	0.300
1.0°	34.2	19.5	0.621	0.095	2.95	0.470	0.129
2.5°	4.66	2.36	0.116	0.032	0.550	0.094	0.049
WBLE 60 GeV at 1300 km with decay pipe 2m radius 380 m length							
0°	151.0	69.2	1.34	0.169	7.83	2.53	0.403
0.5°	77.2	28.7	0.906	0.134	5.33	1.52	0.305
1.0°	33.3	18.4	0.520	0.098	3.08	0.480	0.141
2.5°	5.05	2.56	0.120	0.035	0.611	0.105	0.058
WBLE 40 GeV at 1300 km with decay pipe 2m radius 380 m length							
0°	110.4	44.4	1.02	0.159	6.50	2.05	0.357
WBLE 28 GeV at 1300 km with decay pipe 2m radius 180 m length							
0°	52.5	19.4	0.374	0.074	3.87	1.05	0.223

TABLE III: Signal and background interaction rates at 1300 Km (Fermilab-HOMESTAKE) using different WBLE beam energies and off-axis angles. The rates integrated over the neutrino energy range of 0 - 20 GeV. Rates are given per MW.10^7s.kT. For $\nu_\mu \to \nu_e$ oscillations a value of $\sin^2 2\theta_{13} = 0.04$ and $\Delta m^2_{31} = 2.5 \times 10^{-3}$ eV^2 is used. No detector model is used.

Degrees off-axis	$\bar{\nu}_\mu$ CC	$\bar{\nu}_\mu$ CC osc	$\bar{\nu}_e$ CC beam	$\bar{\nu}_e$ QE beam	NC-1π^0	$\bar{\nu}_\mu \to \bar{\nu}_e$ CC	$\bar{\nu}_\mu \to \bar{\nu}_e$ QE
WBLE 120 GeV at 1300 km with decay pipe 2m radius 380 m length							
0°	75.0	37.7	0.570	0.106	7.79	0.669	0.160
0.5°	33.5	13.0	0.356	0.077	4.90	0.332	0.103
1.0°	12.0	6.47	0.185	0.056	2.64	0.122	0.056
2.5°	1.41	0.694	0.037	0.013	0.499	0.033	0.022
WBLE 60 GeV at 1300 km with decay pipe 2m radius 380 m length							
0°	50.5	21.3	0.373	0.088	6.05	0.507	0.137
0.5°	25.4	8.52	0.248	0.066	4.23	0.272	0.094
1.0°	10.3	5.38	0.144	0.045	2.52	0.116	0.058
2.5°	1.36	0.667	0.031	0.013	0.518	0.035	0.024
WBLE 40 GeV at 1300 km with decay pipe 2m radius 380 m length							
0°	33.8	12.5	0.270	0.069	4.70	0.366	0.110
WBLE 28 GeV at 1300 km with decay pipe 2m radius 180 m length							
0°	14.6	4.94	0.076	0.026	2.64	0.172	0.065

TABLE IV: Signal and background anti-neutrino interaction rates at 1300 Km (Fermilab-HOMESTAKE) using different WBLE beam energies and off-axis angles. The rates integrated over the neutrino energy range of 0 - 20 GeV. Rates are given per MW.10^7s.kT. For $\nu_\mu \to \nu_e$ oscillations a value of $\sin^2 2\theta_{13} = 0.04$ and $\Delta m^2_{31} = 2.5 \times 10^{-3}$ eV^2 is used. No detector model is used.

		Neutrino Rates				Anti Neutrino Rates			
Beam (mass ordering)	$\sin^2 2\theta_{13}$	δ_{CP} deg.							
		0°	90°	180°	270°	0°	90°	180°	270°
NuMI LE 12 km offaxs (+)	0.02	76	108	69	36	20	7.7	17	30
NuMI LE 12 km offaxs (-)	0.02	46	77	52	21	28	14	28	42
NuMI LE 12 km offaxs (+)	0.1	336	408	320	248	86	57	78	106
NuMI LE 12 km offaxs (-)	0.1	210	280	224	153	125	95	126	157
NuMI LE 40 km offaxs (+)	0.02	5.7	8.8	5.1	2.2	2.5	1.6	0.7	3.3
NuMI LE 40 km offaxs (-)	0.02	4.2	8.0	5.7	2.0	2.3	2.2	0.8	3.6
NuMI LE 40 km offaxs (+)	0.1	17	24	15	9.4	6.7	2.8	4.6	8.5
NuMI LE 40 km offaxs (-)	0.1	12	21	16	7.7	6.6	3.4	6.4	9.6
WBLE 1300 km (+)	0.02	141	192	128	77	19	11	18	36
WBLE 1300 km (-)	0.02	58	111	88	35	45	25	45	64
WBLE 1300 km (+)	0.1	607	720	579	467	106	67	83	122
WBLE 1300 km (-)	0.1	269	388	335	216	196	154	196	240
WBLE 2500 km (+)	0.02	61	103	88	46	11	4.6	4.7	11
WBLE 2500 km (-)	0.02	16	36	33	13	28	15	18	31
WBLE 2500 km (+)	0.1	270	361	328	238	27	13	13	28
WBLE 2500 km (-)	0.1	47	92	85	39	103	74	80	109

TABLE V: This table contains signal event rates after $\nu_\mu \rightarrow \nu_e$ conversion for the various scenarios described. The event rates here have no detector model or backgrounds. The units are charged current events per 100 kTon of detector mass for 1 MW of beam for $10^7 sec$ of operation. For NuMI running we assume 120 GeV protons in the LE tune and for WBLE we have assumed 60 GeV protons. The charged current cross sections applied as well as the oscillation parameters used are described in the text.

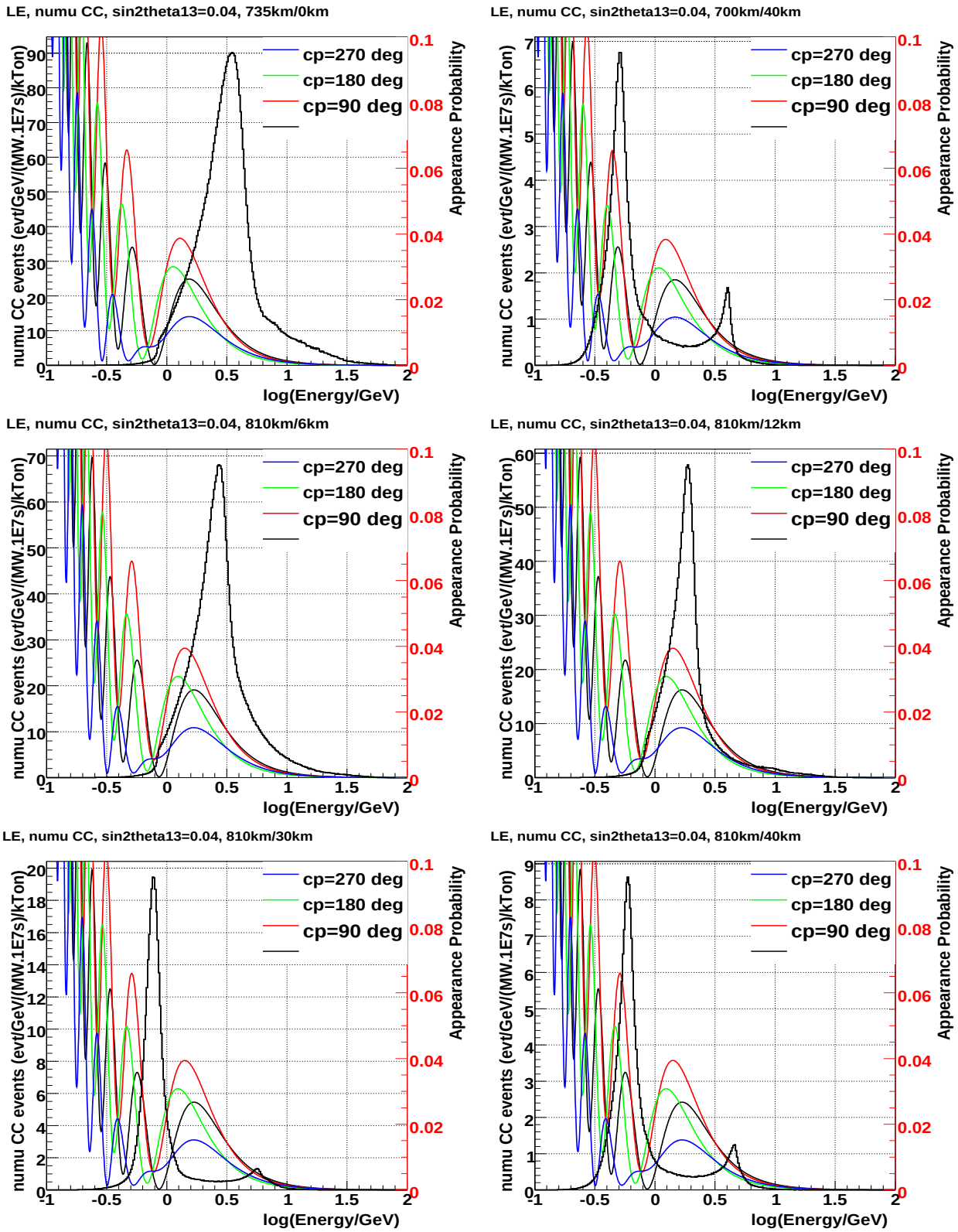

FIG. 1: NuMI total CC event spectra (no oscillations) with the $\nu_\mu \rightarrow \nu_e$ oscillation probabilities overlaid for $\sin^2 2\theta_{13} = 0.04$ and various values of δ_{cp} as a function of $\log(\mathrm{E}_\nu)$.

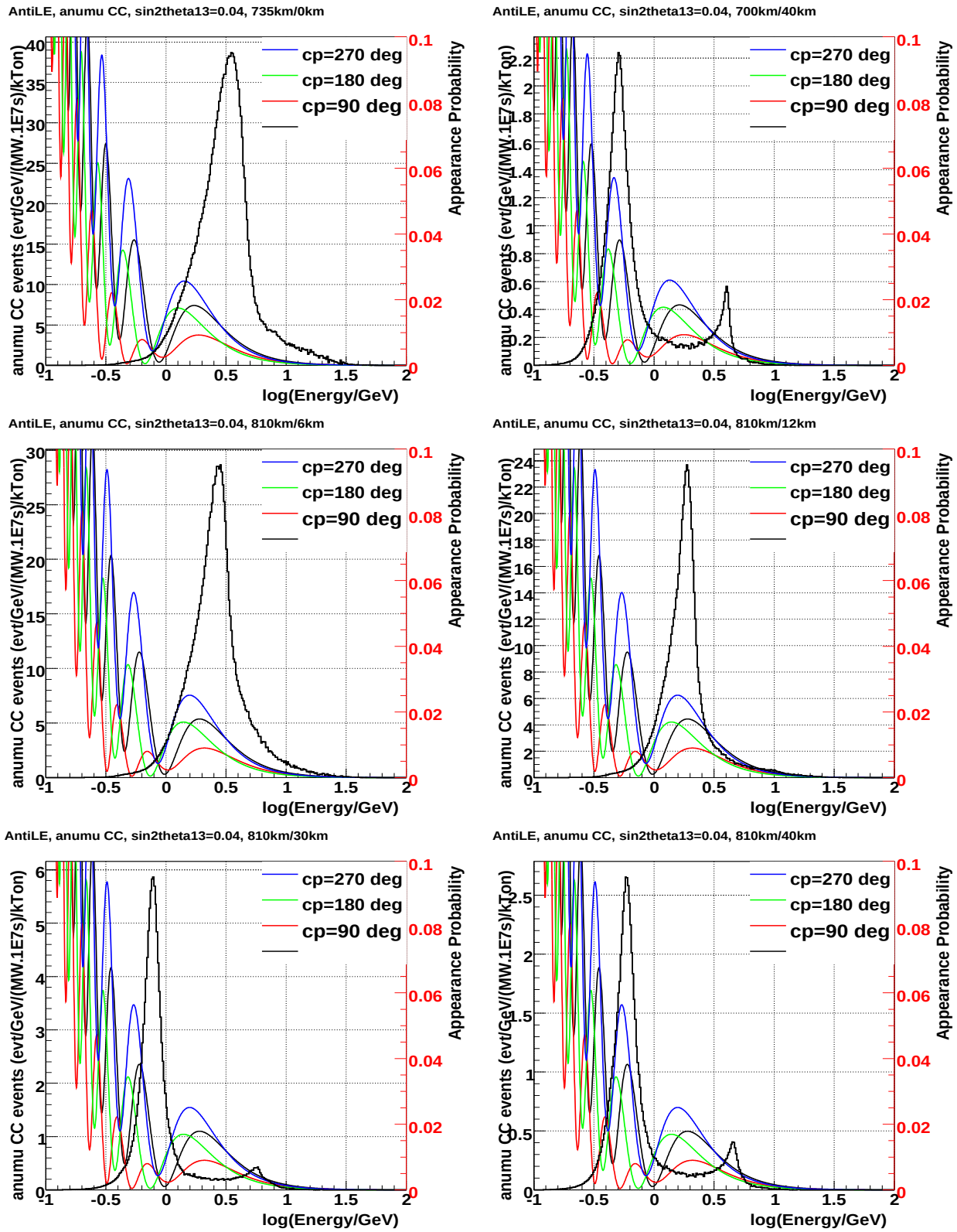

FIG. 2: NuMI total CC event spectra (no oscillations) with the $\bar{\nu}_\mu \rightarrow \bar{\nu}_e$ oscillation probabilities overlaid for $\sin^2 2\theta_{13} = 0.04$ and various values of δ_{cp} as a function of $\log(\mathrm{E}_\nu)$.

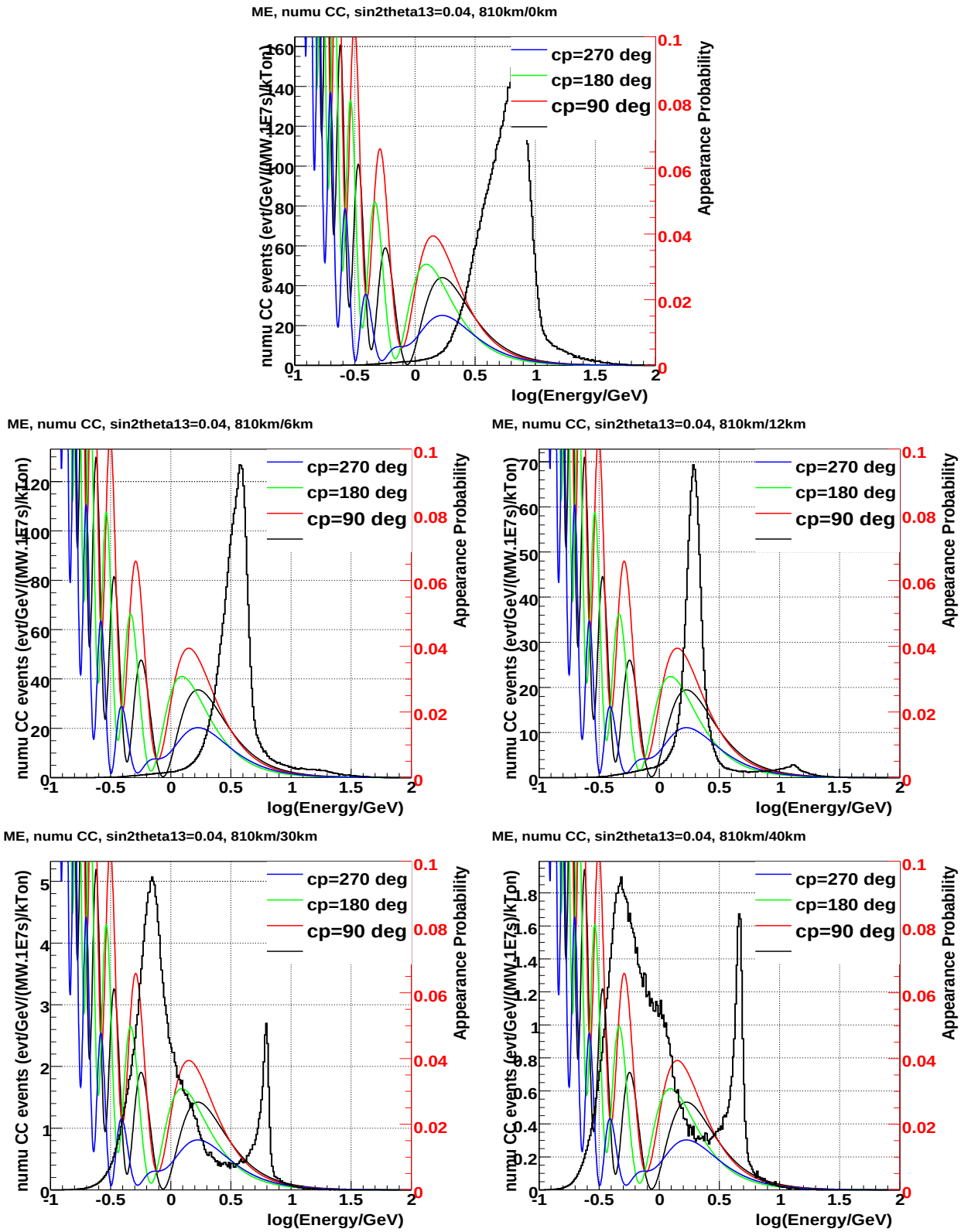

FIG. 3: NuMI total CC event spectra (no oscillations) with the $\nu_\mu \rightarrow \nu_e$ oscillation probabilities overlaid for $\sin^2 2\theta_{13} = 0.04$ and various values of δ_{cp} as a function of $\log(\mathrm{E}_\nu)$.

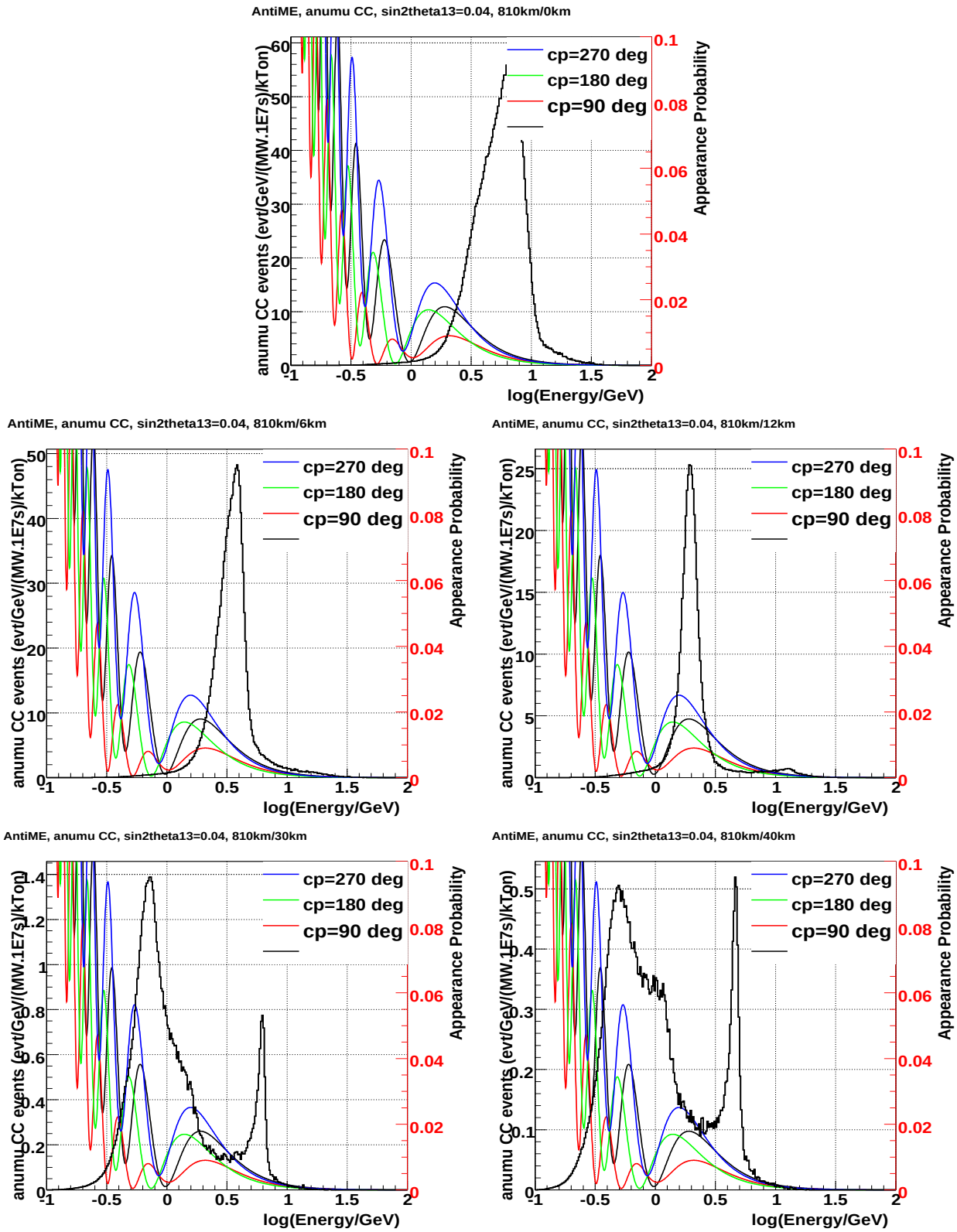

FIG. 4: NuMI total anti ν CC event spectra (no oscillations) with the $\bar{\nu_\mu} \rightarrow \bar{\nu_e}$ oscillation probabilities overlaid for $\sin^2 2\theta_{13} = 0.04$ and various values of δ_{cp} as a function of $\log(\mathrm{E}_\nu)$.

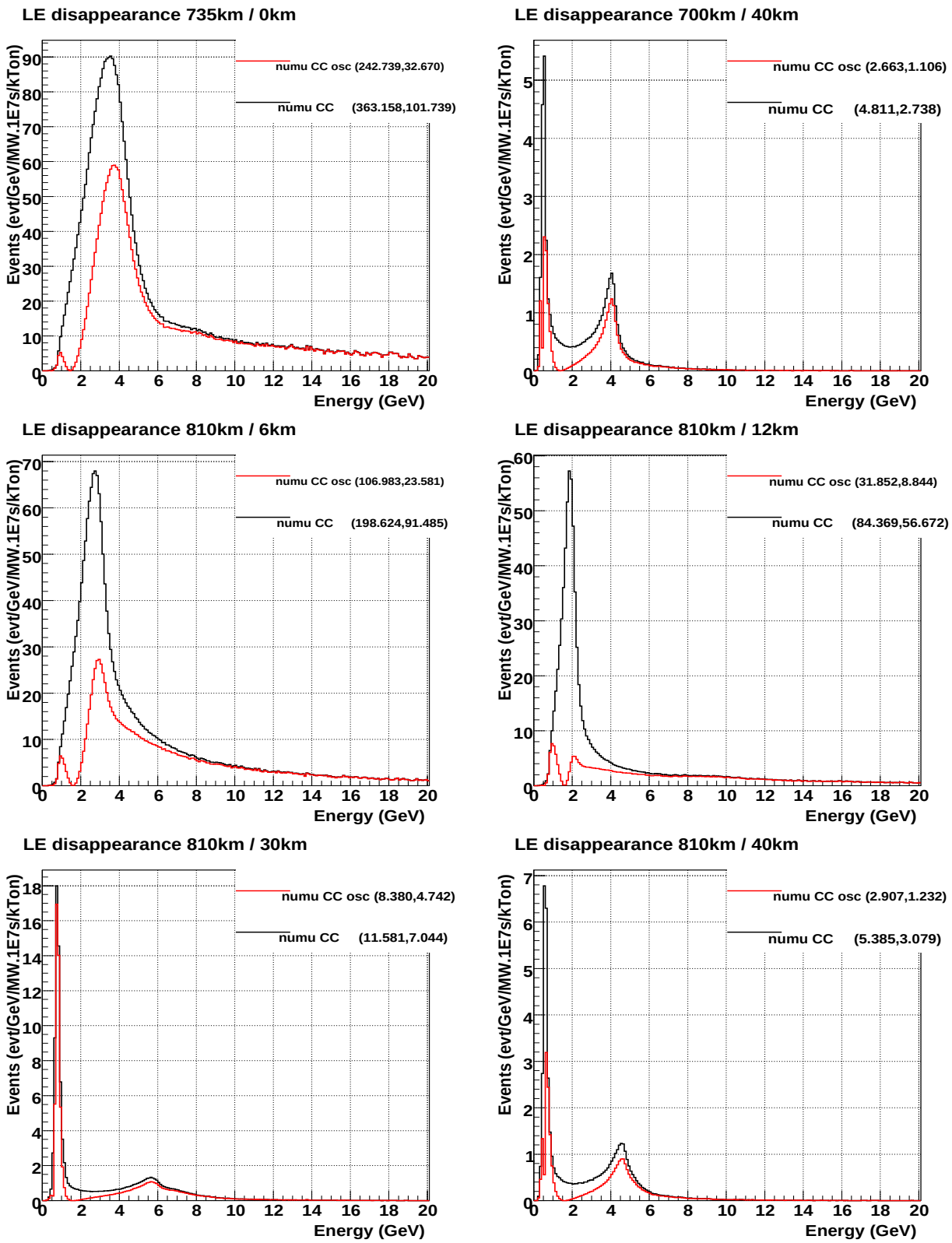

FIG. 5: $\nu_\mu \to \nu_\mu$ total CC interaction rates for NuMI LE tune and various off-axis options for (0-20 GeV, 0-3GeV).

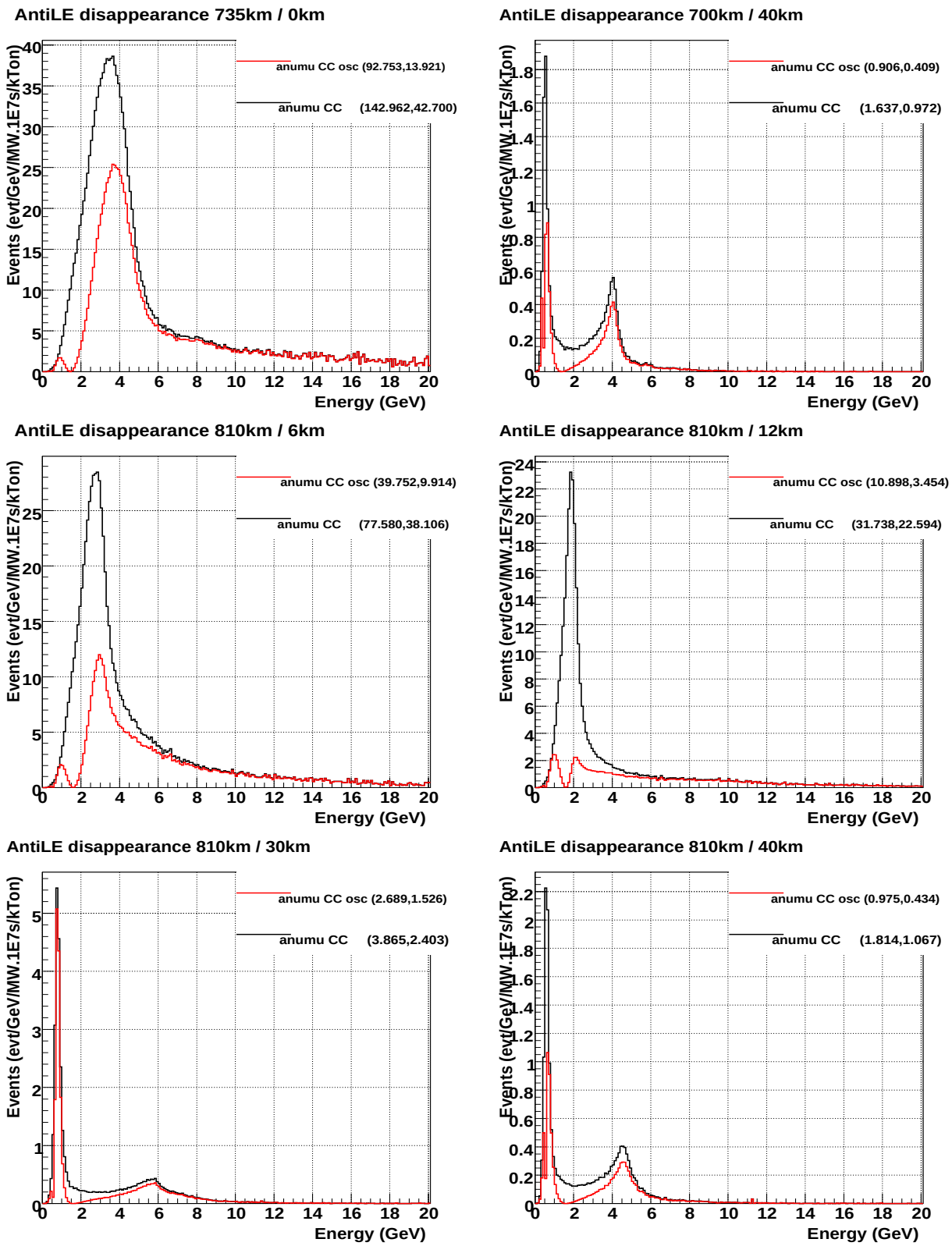

FIG. 6: $\bar{\nu}_\mu \rightarrow \bar{\nu}_\mu$ total CC interaction rates for NuMI LE tune and various off-axis options for (0-20 GeV, 0-3GeV).

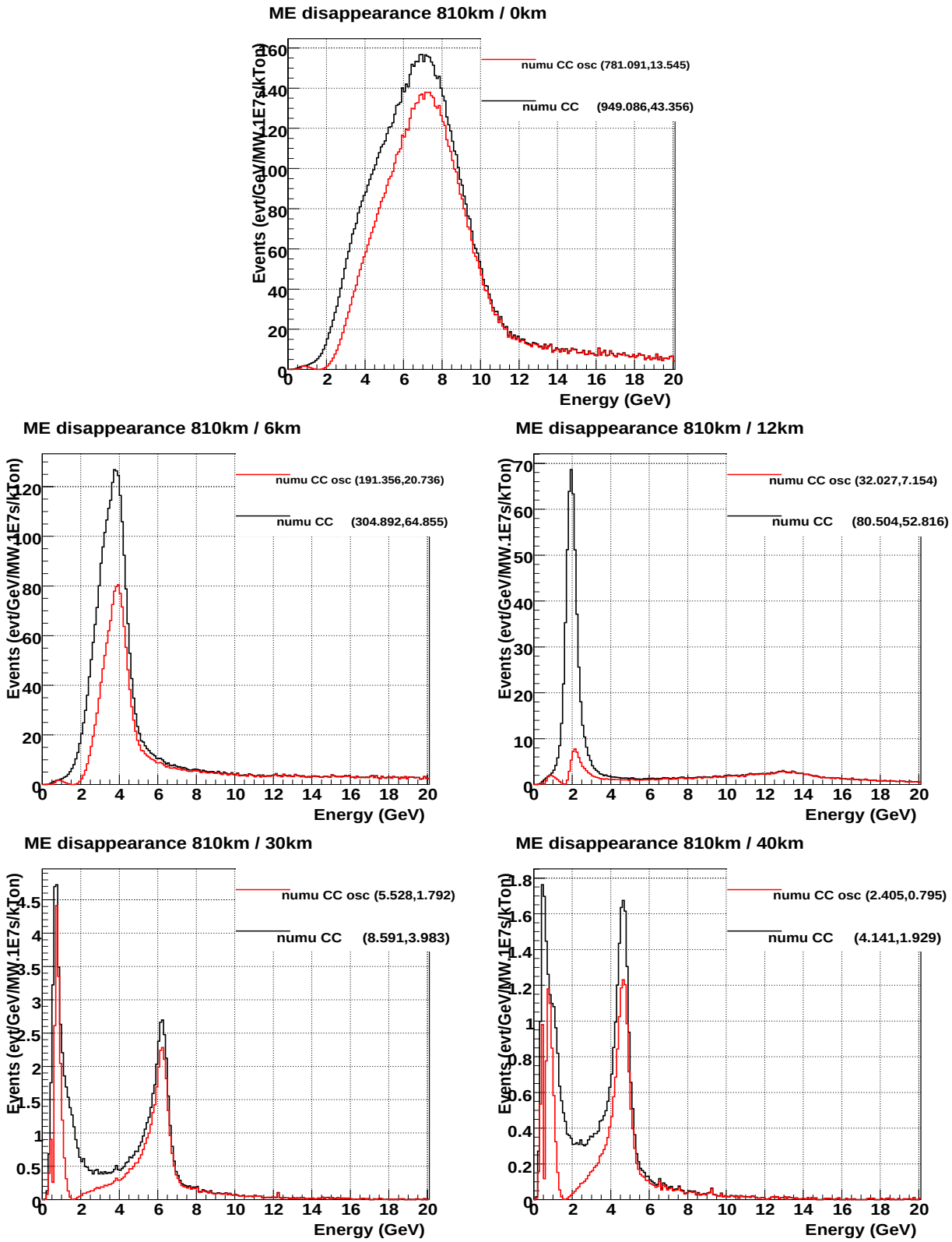

FIG. 7: $\nu_\mu \rightarrow \nu_\mu$ total CC interaction rates for NuMI ME tune and various off-axis options for (0-20 GeV, 0-3GeV).

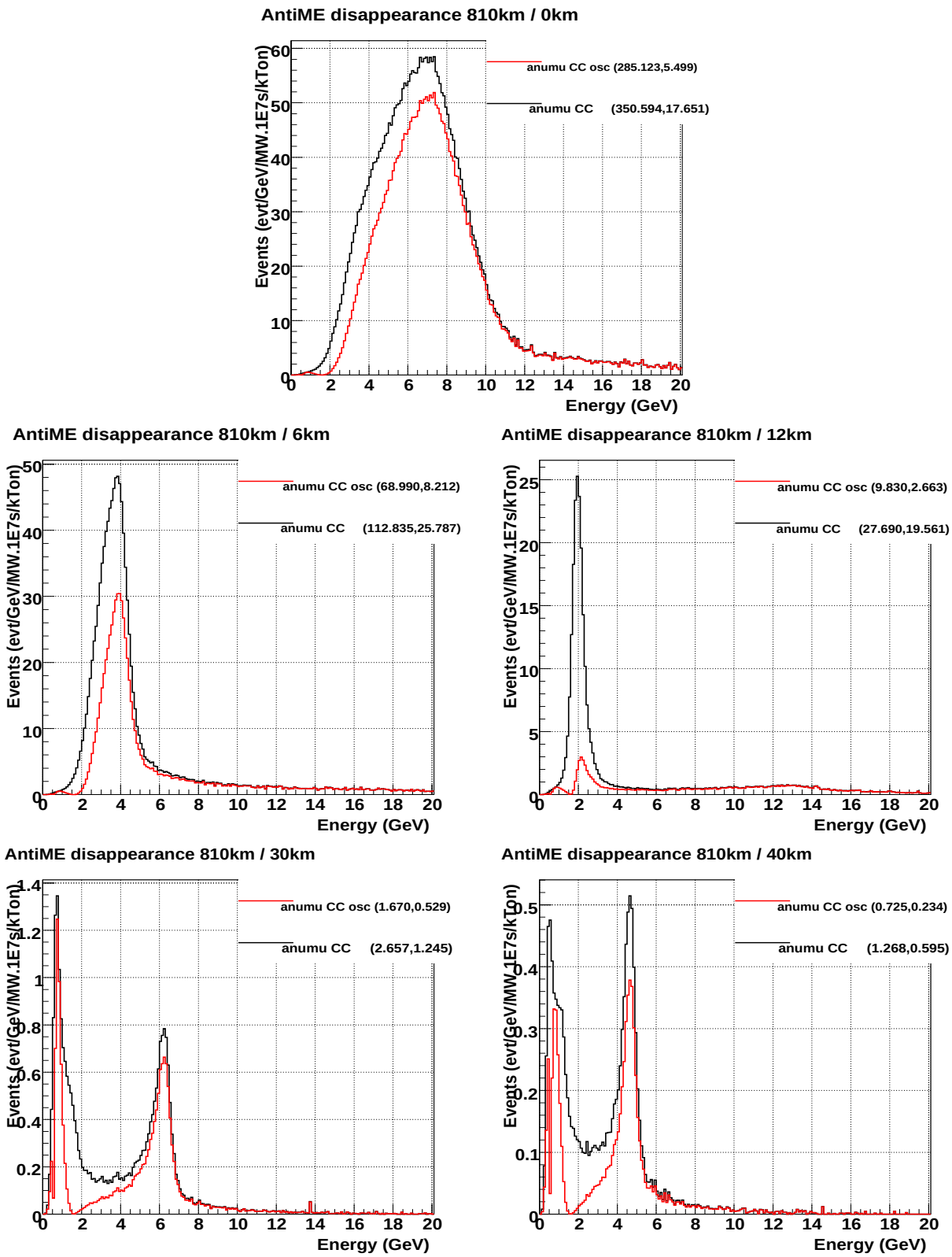

FIG. 8: $\bar{\nu_\mu} \rightarrow \bar{\nu_\mu}$ total CC interaction rates for NuMI ME tune and various off-axis options for (0-20 GeV, 0-3GeV).

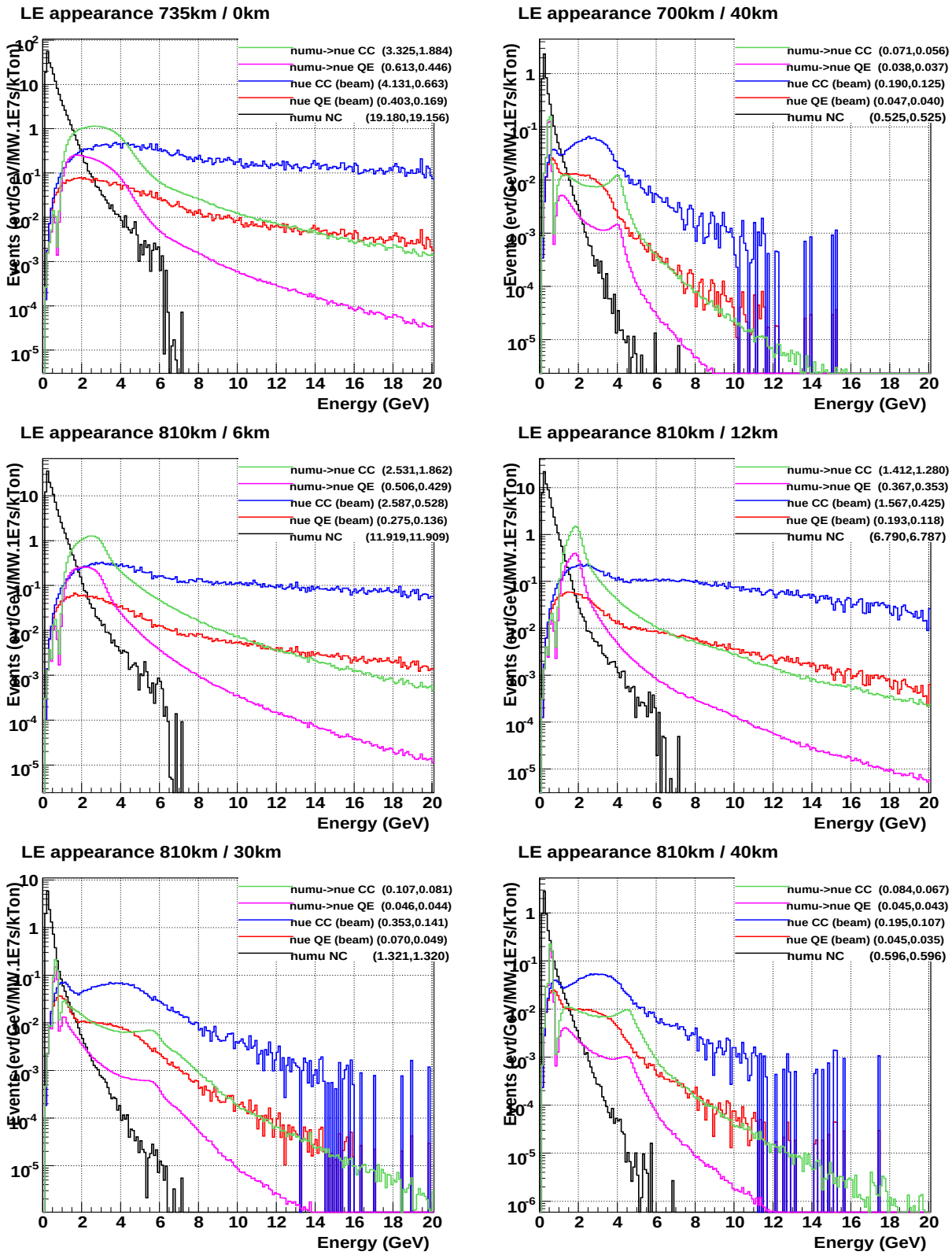

FIG. 9: $\nu_\mu \rightarrow \nu_e$ CC interaction rates for NuMI LE tune and various off-axis options for (0-20 GeV, 0-3GeV).

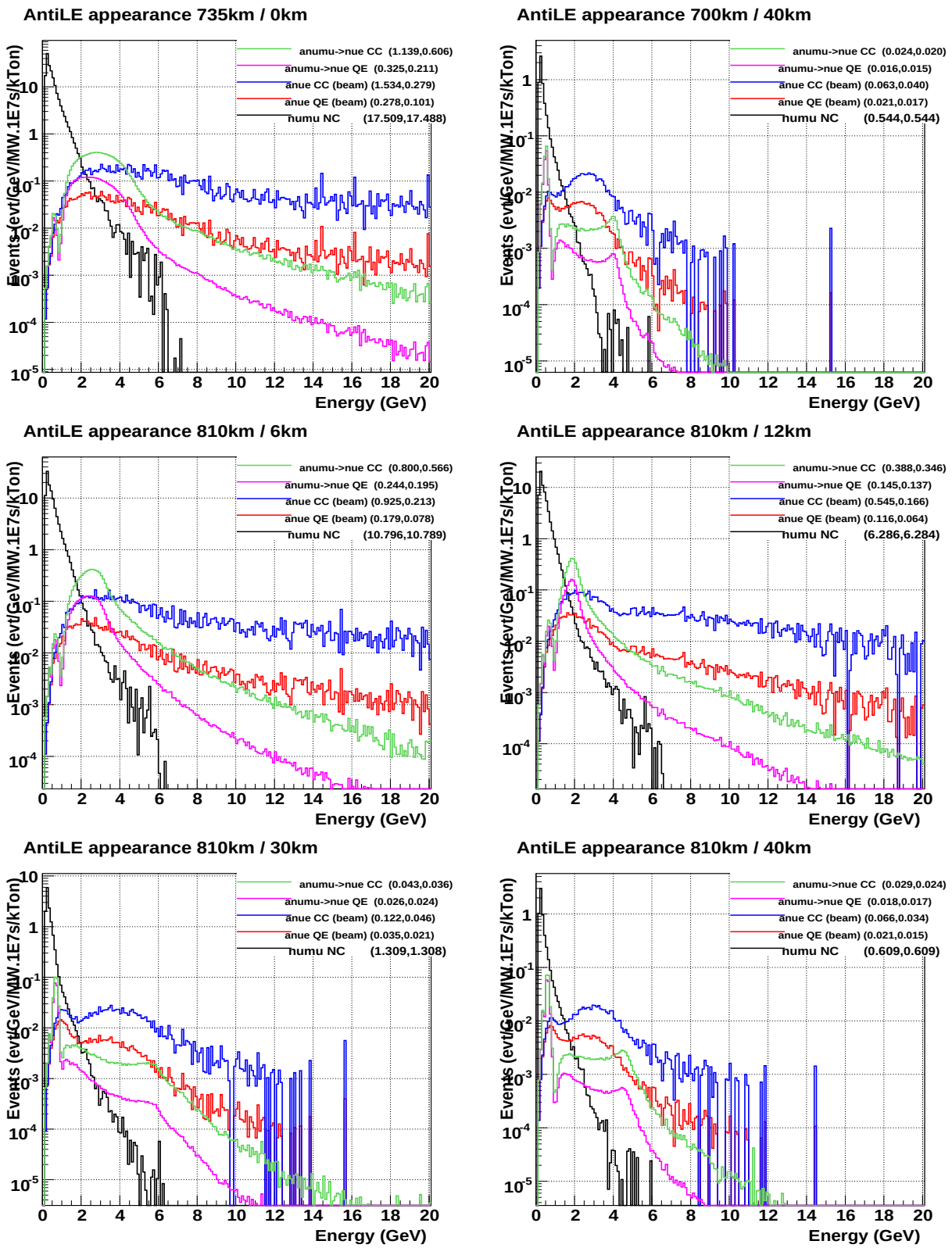

FIG. 10: $\bar{\nu}_\mu \rightarrow \bar{\nu}_e$ CC interaction rates for NuMI LE tune and various off-axis options for (0-20 GeV, 0-3GeV).

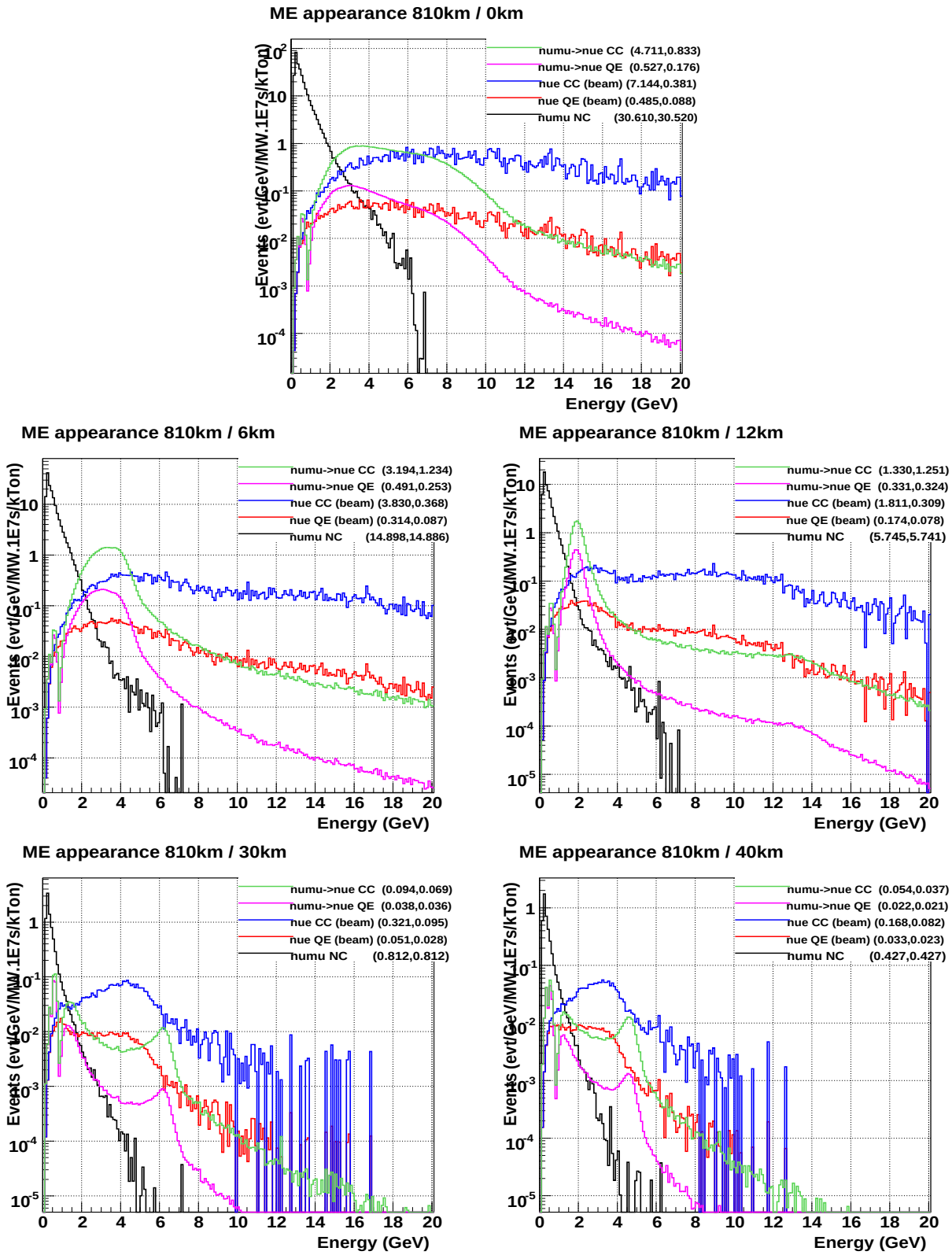

FIG. 11: $\nu_\mu \rightarrow \nu_e$ total CC interaction rates for NuMI ME tune and various off-axis options for (0-20 GeV, 0-3GeV).

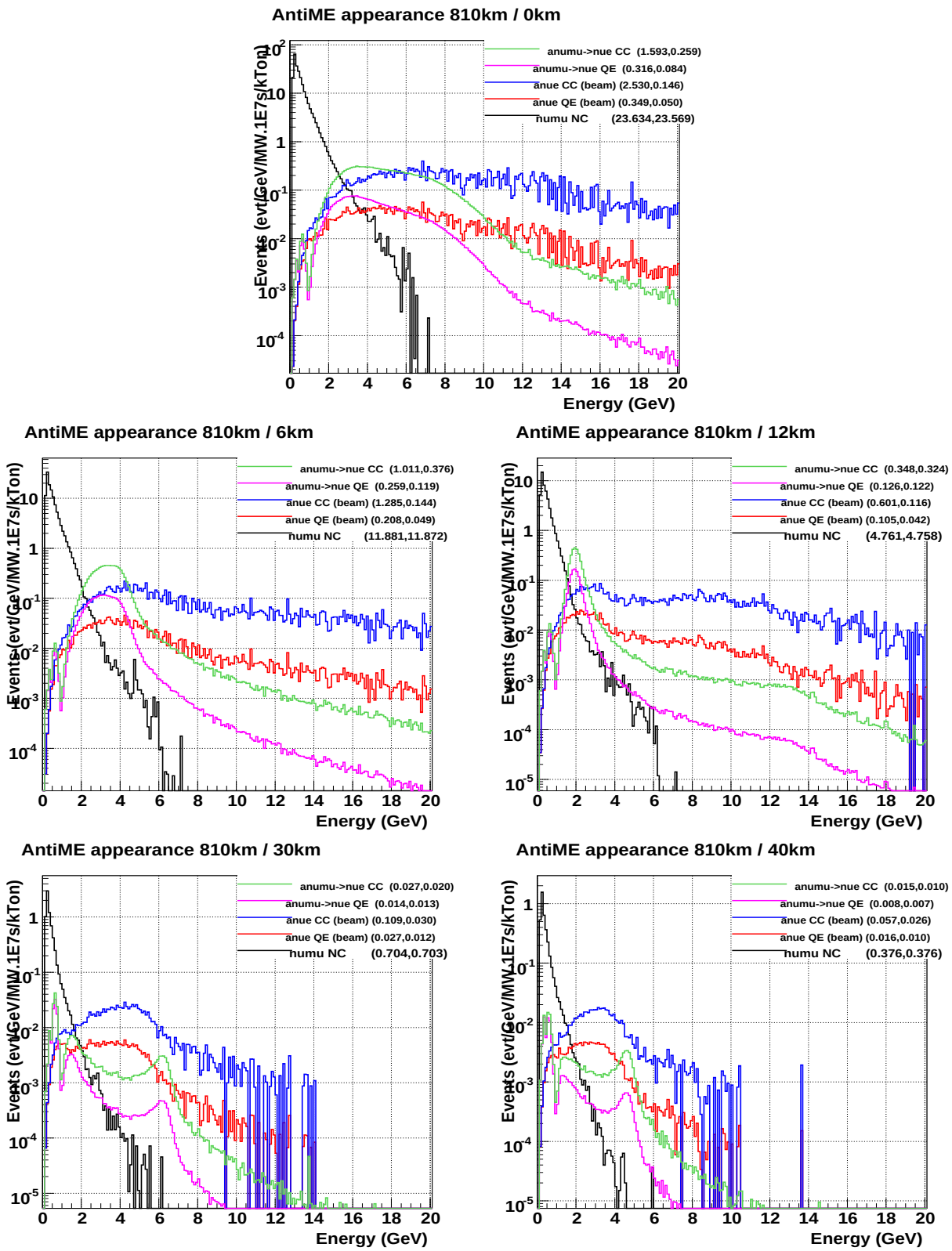

FIG. 12: $\bar{\nu}_\mu \rightarrow \bar{\nu}_e$ CC interaction rates for NuMI ME tune and various off-axis options for (0-20 GeV, 0-3GeV).

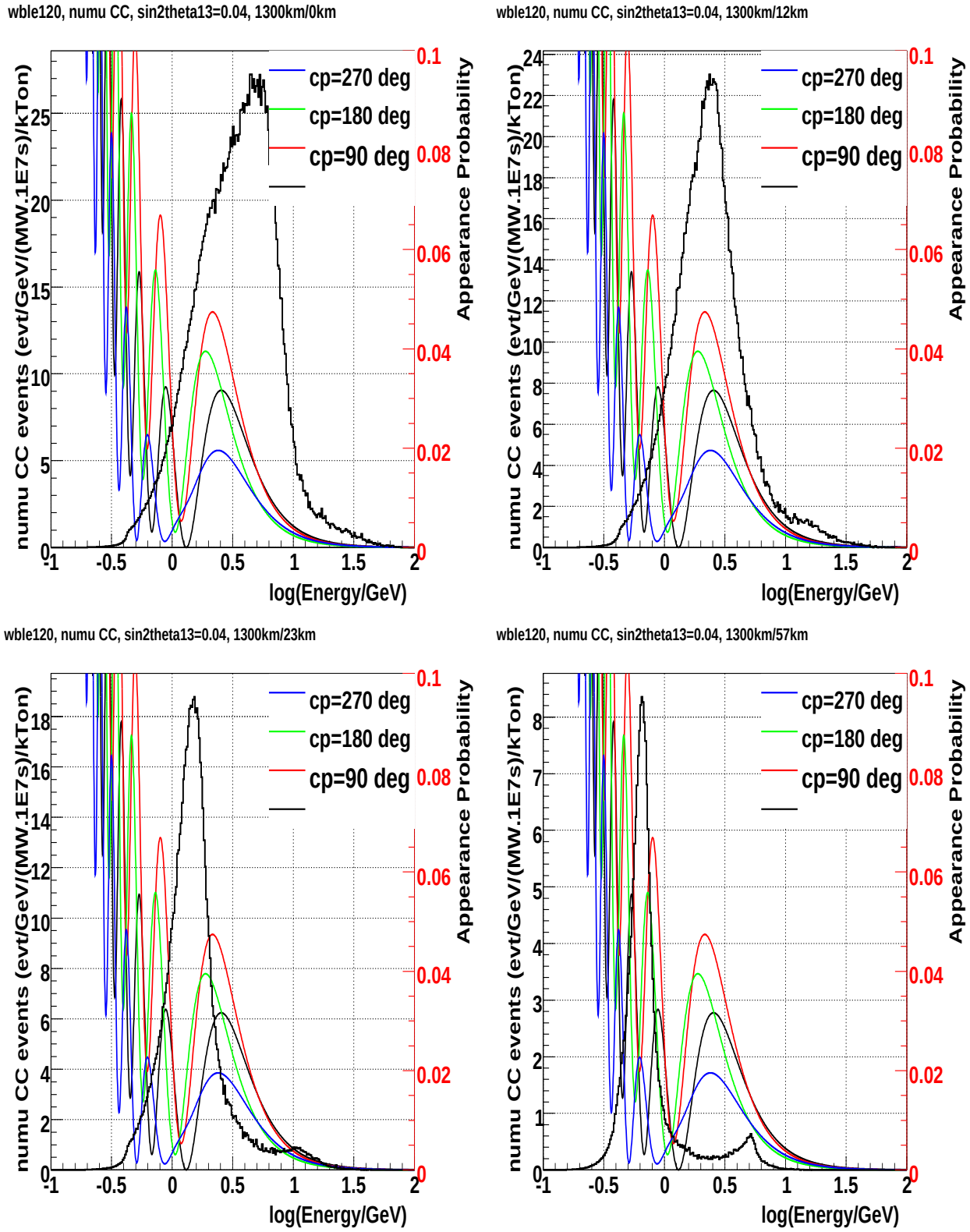

FIG. 13: WBLE total CC event spectra (no oscillations) with the $\nu_\mu \to \nu_e$ oscillation probabilities overlaid for $\sin^2 2\theta_{13} = 0.04$ and various values of δ_{cp} as a function of $\log(\mathrm{E}_\nu)$.

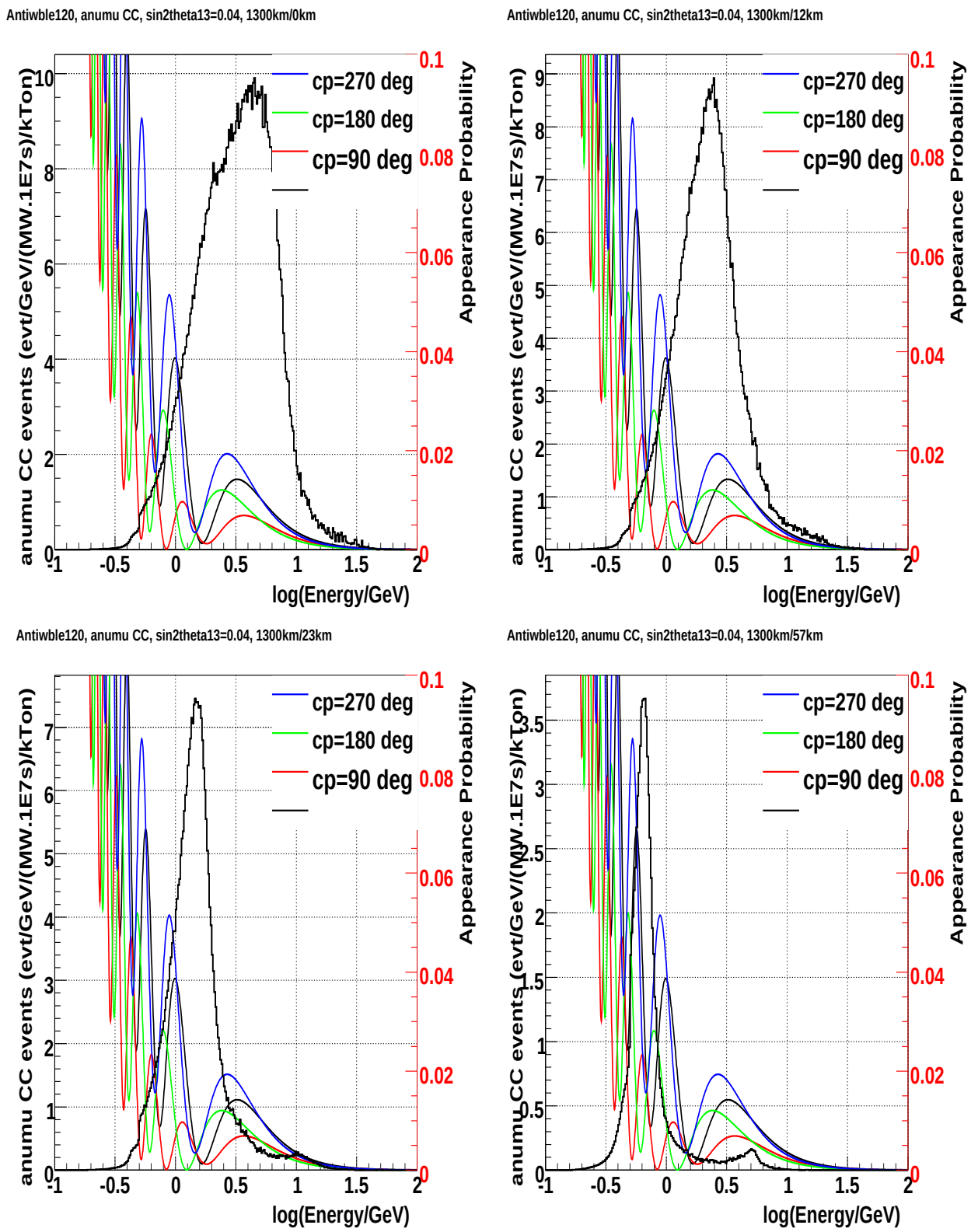

FIG. 14: WBLE total CC event spectra (no oscillations) with the $\bar{\nu}_\mu \rightarrow \bar{\nu}_e$ oscillation probabilities overlaid for $\sin^2 2\theta_{13} = 0.04$ and various values of δ_{cp} as a function of $\log(\mathrm{E}_\nu)$.

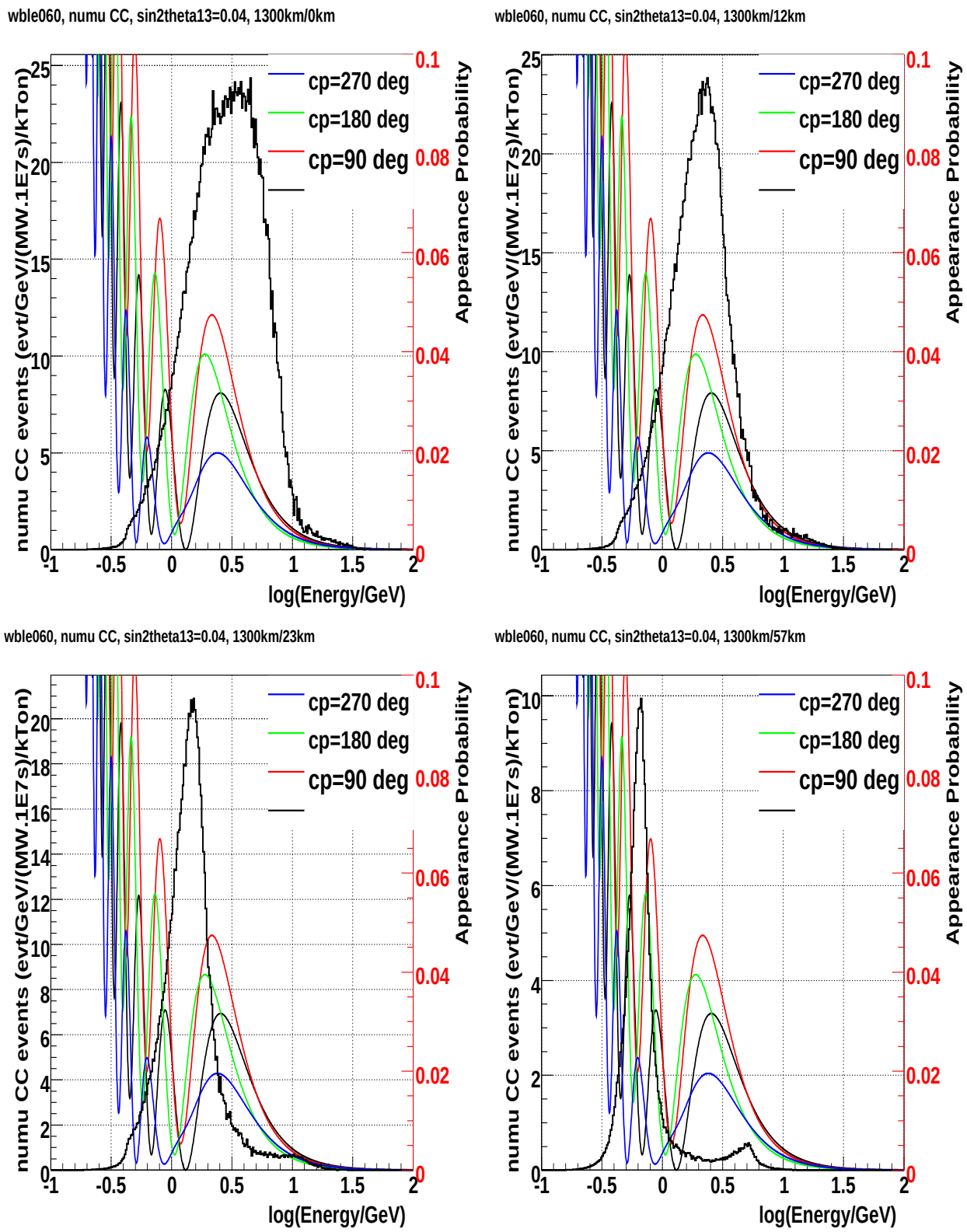

FIG. 15: WBLE total CC event spectra (no oscillations) with the $\nu_\mu \to \nu_e$ oscillation probabilities overlaid for $\sin^2 2\theta_{13} = 0.04$ and various values of δ_{cp} as a function of $\log(\mathrm{E}_\nu)$.

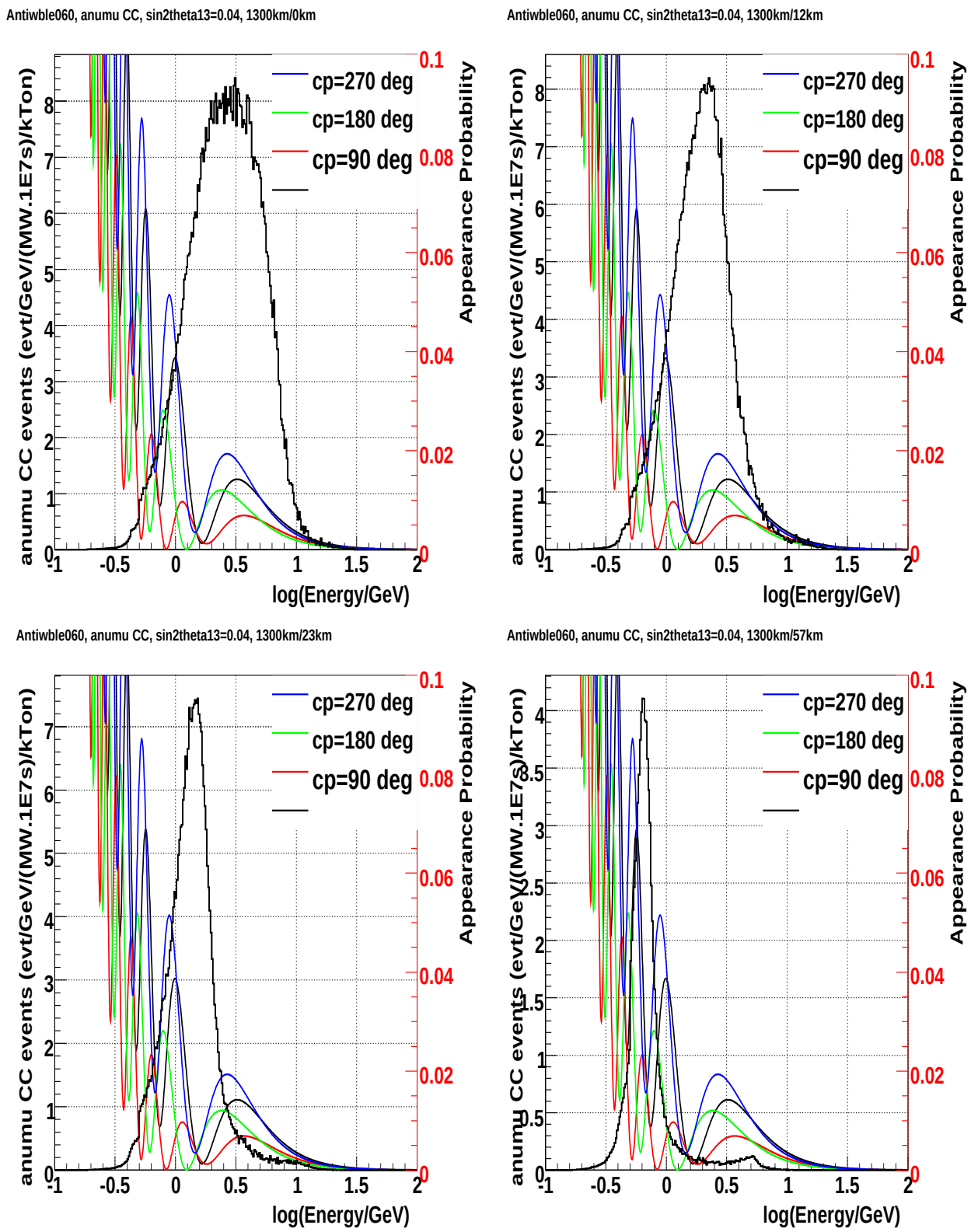

FIG. 16: WBLE total CC event spectra (no oscillations) with the $\bar{\nu}_\mu \to \bar{\nu}_e$ oscillation probabilities overlaid for $\sin^2 2\theta_{13} = 0.04$ and various values of δ_{cp} as a function of $\log(\mathrm{E}_\nu)$.

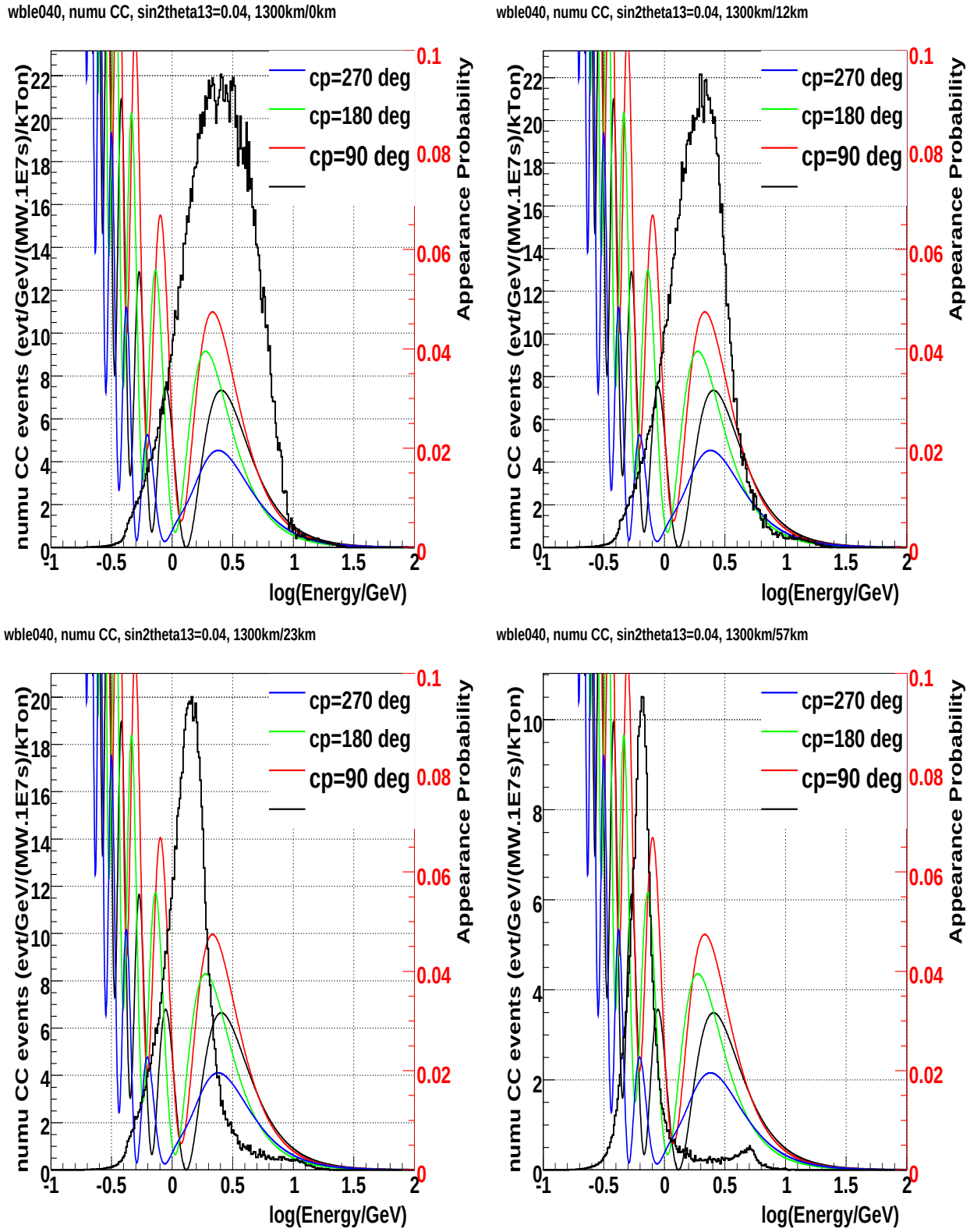

FIG. 17: WBLE total CC event spectra (no oscillations) with the $\nu_\mu \to \nu_e$ oscillation probabilities overlaid for $\sin^2 2\theta_{13} = 0.04$ and various values of δ_{cp} as a function of $\log(\mathrm{E}_\nu)$.

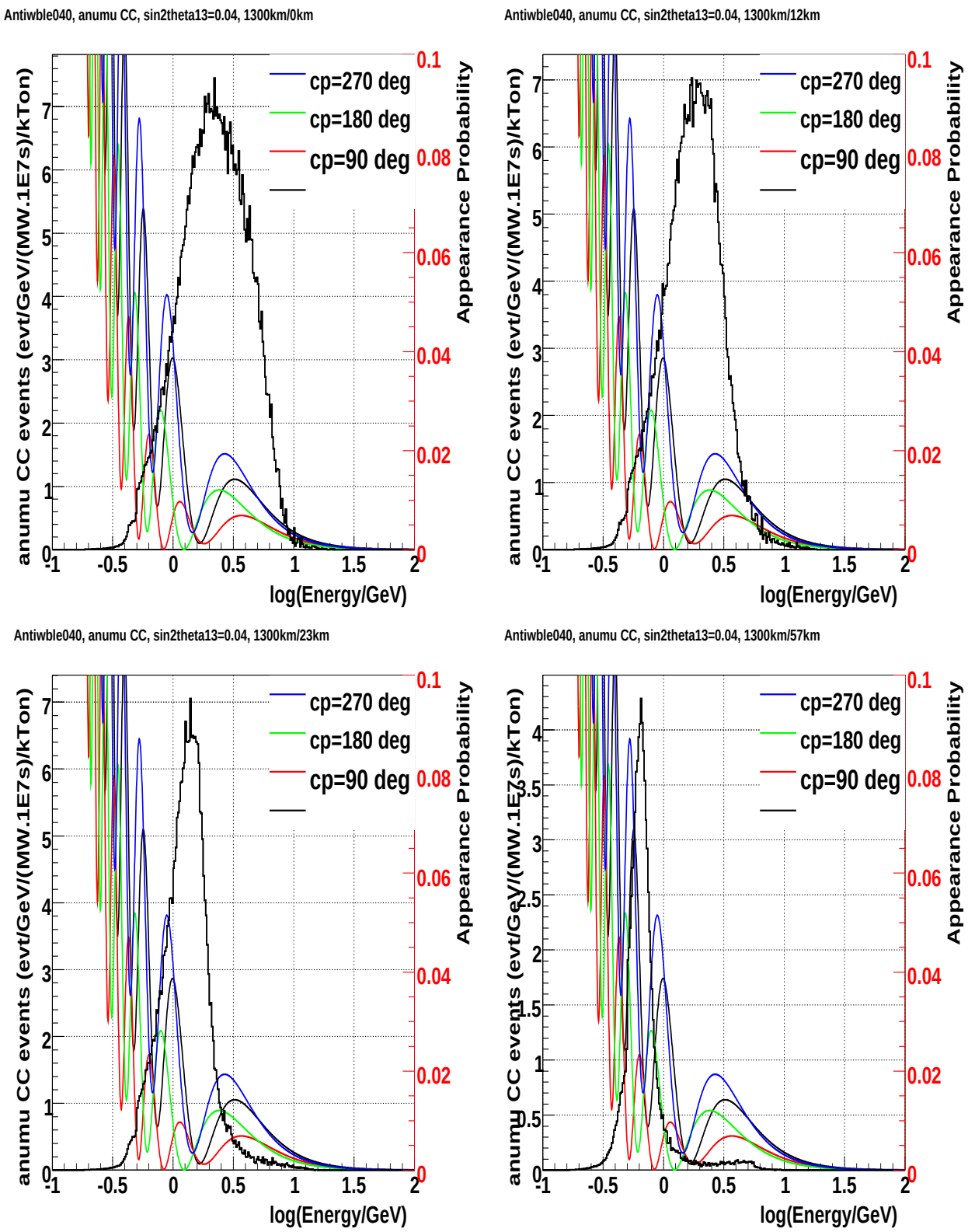

FIG. 18: WBLE total CC event spectra (no oscillations) with the $\bar{\nu}_\mu \to \bar{\nu}_e$ oscillation probabilities overlaid for $\sin^2 2\theta_{13} = 0.04$ and various values of δ_{cp} as a function of $\log(\mathrm{E}_\nu)$.

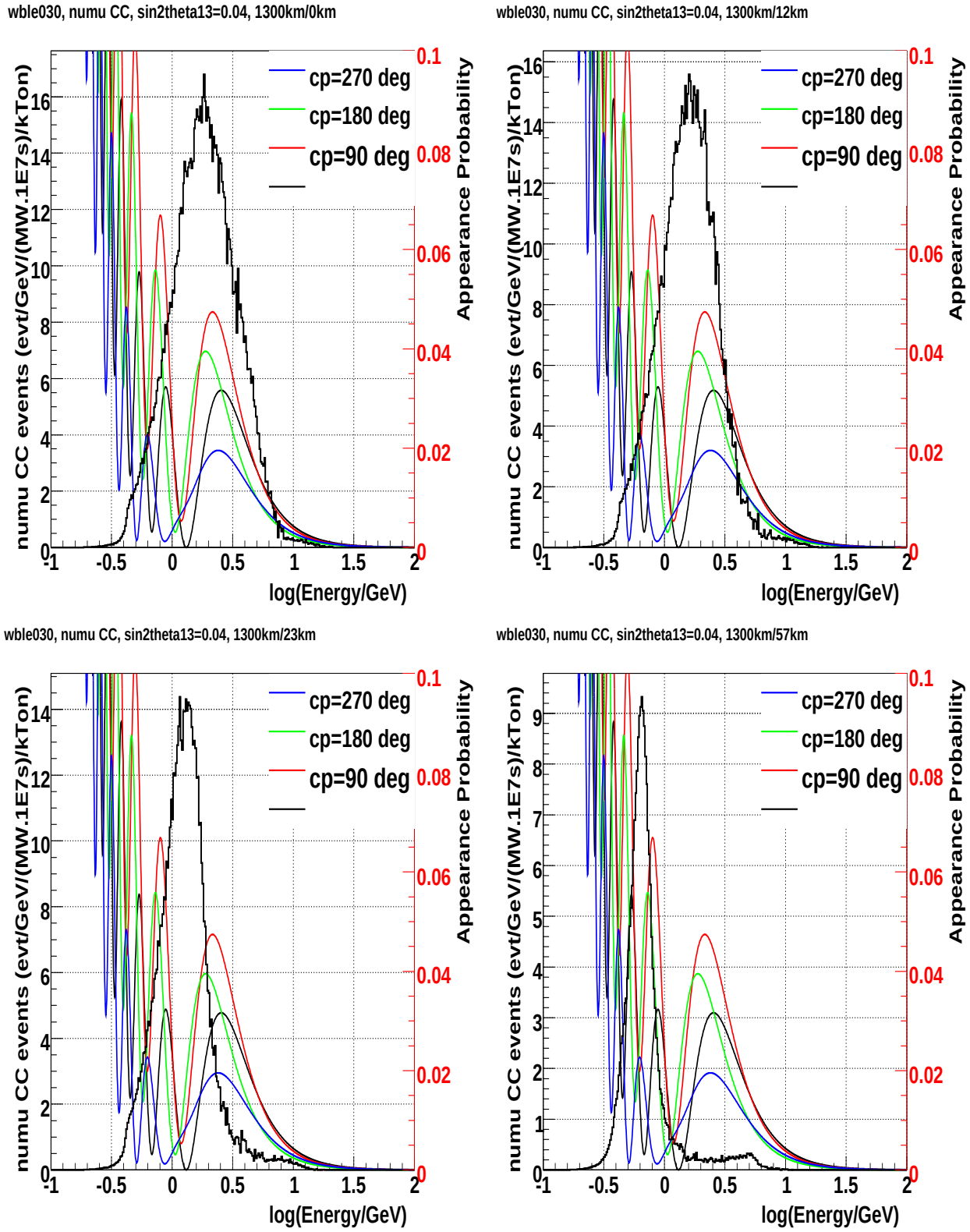

FIG. 19: WBLE total CC event spectra (no oscillations) with the $\nu_\mu \to \nu_e$ oscillation probabilities overlaid for $\sin^2 2\theta_{13} = 0.04$ and various values of δ_{cp} as a function of $\log(\mathrm{E}_\nu)$.

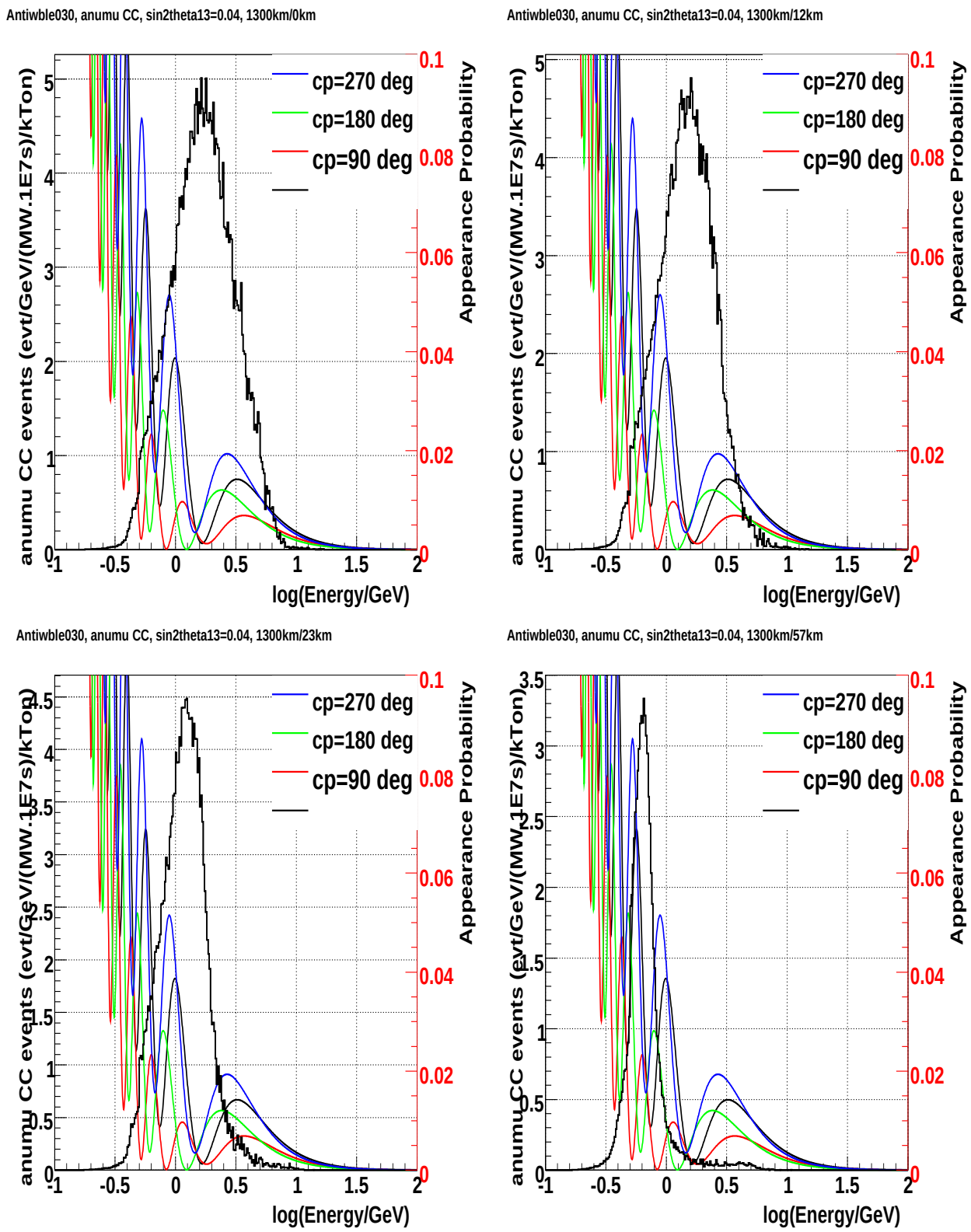

FIG. 20: WBLE total CC event spectra (no oscillations) with the $\bar{\nu}_\mu \rightarrow \bar{\nu}_e$ oscillation probabilities overlaid for $\sin^2 2\theta_{13} = 0.04$ and various values of δ_{cp} as a function of $\log(\mathrm{E}_\nu)$.

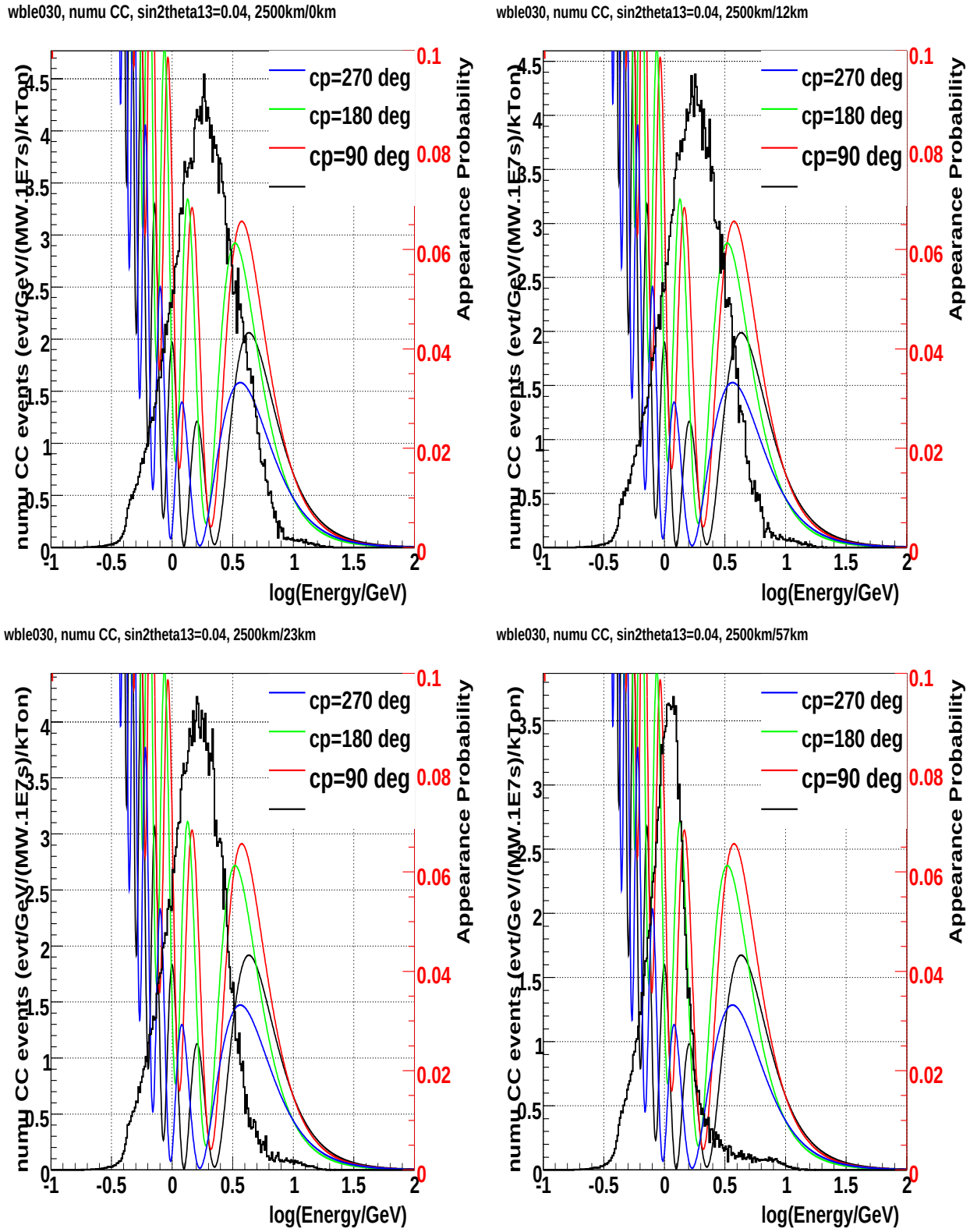

FIG. 21: WBLE total CC event spectra (no oscillations) with the $\nu_\mu \rightarrow \nu_e$ oscillation probabilities overlaid for $\sin^2 2\theta_{13} = 0.04$ and various values of δ_{cp} as a function of $\log(E_\nu)$. For a distance 2500km from the target

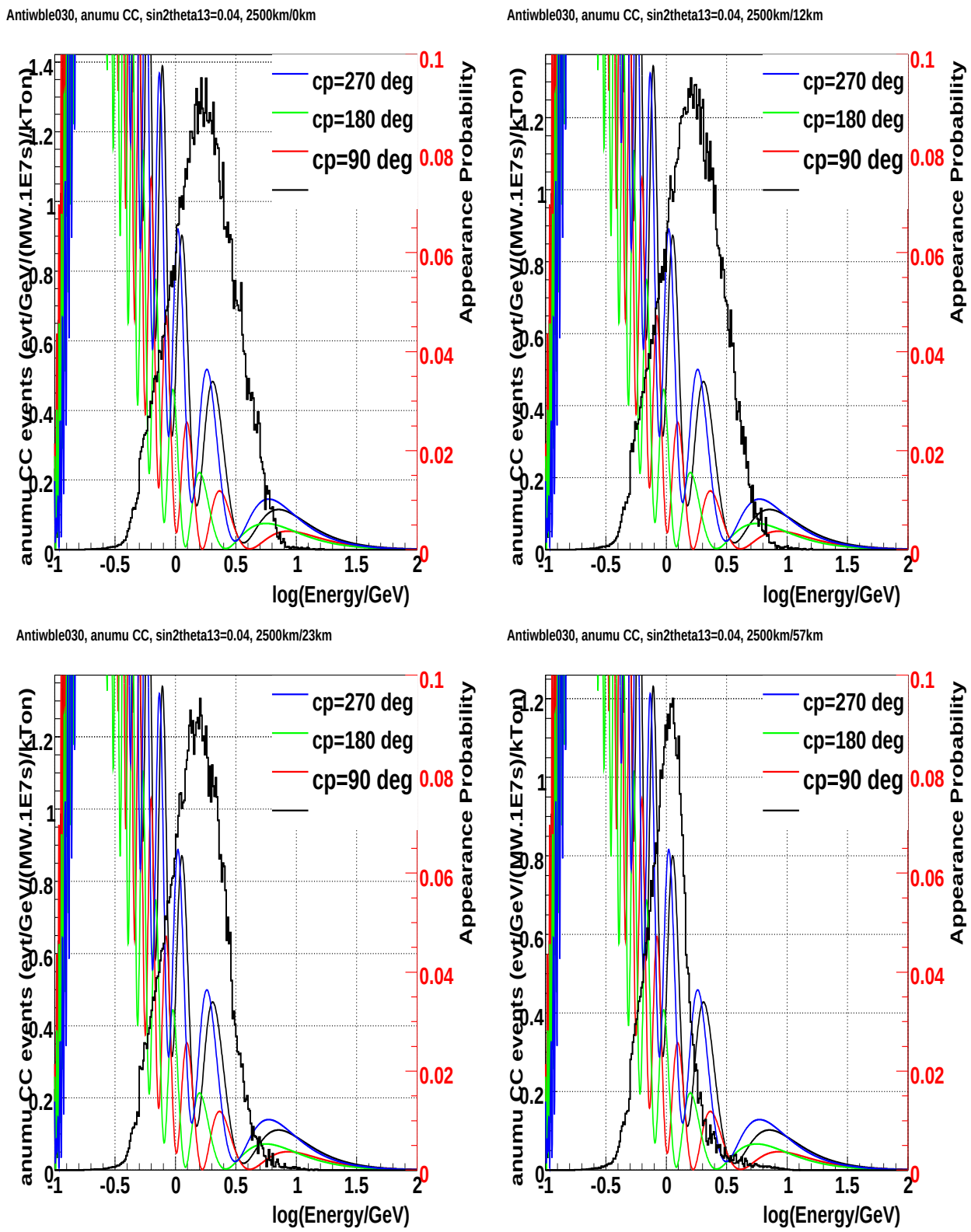

FIG. 22: WBLE total anti nu_μ CC event spectra (no oscillations) with the $\bar{\nu_\mu} \rightarrow \bar{\nu_e}$ oscillation probabilities overlaid for $\sin^2 2\theta_{13} = 0.04$ and various values of δ_{cp} as a function of $\log(\mathrm{E}_\nu)$. For a distance 2500km from the target

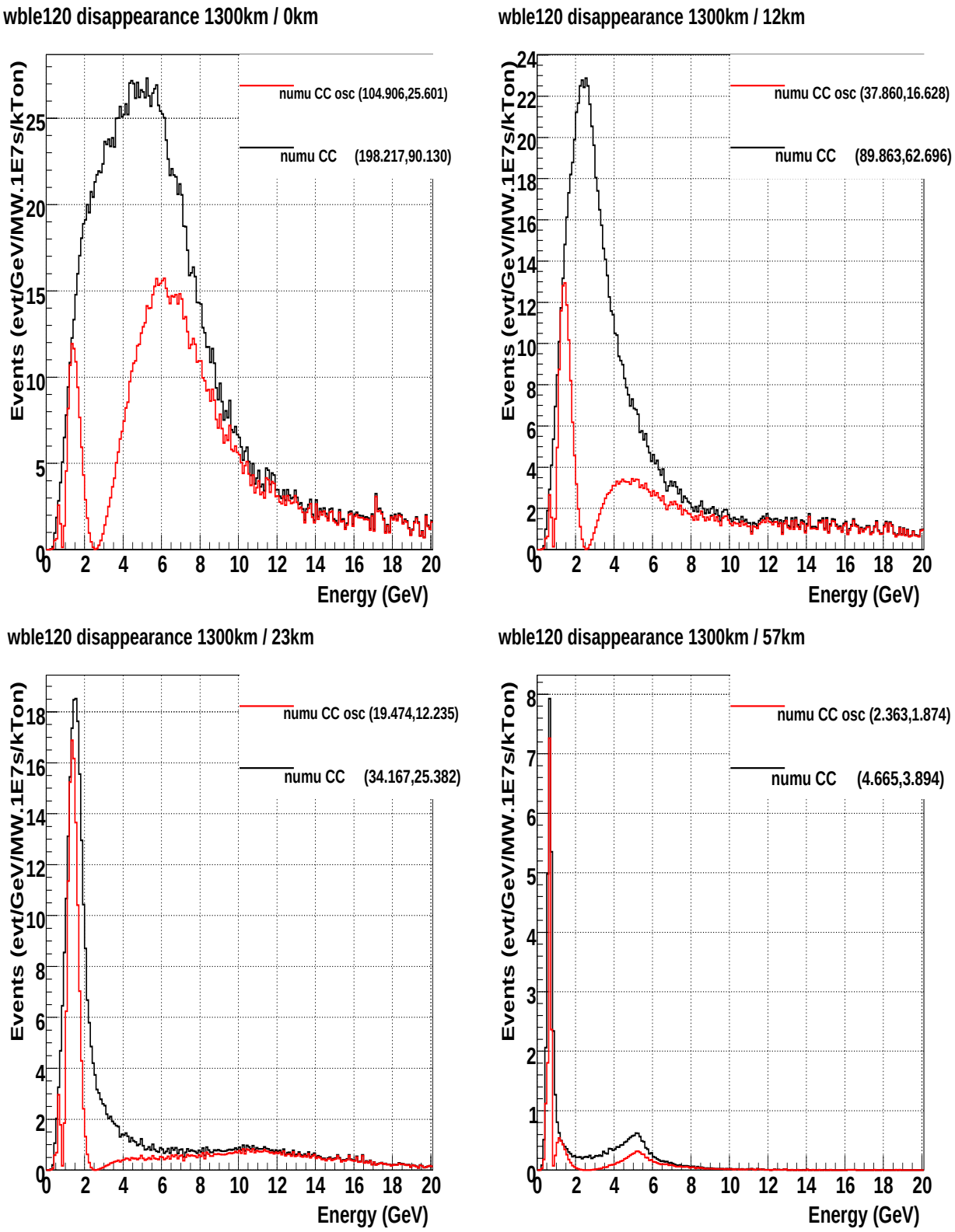

FIG. 23: $\nu_\mu \rightarrow \nu_\mu$ total CC interaction rates for a 120 GeV WBLE beam with various off-axis options for (0-20 GeV, 0-5GeV).

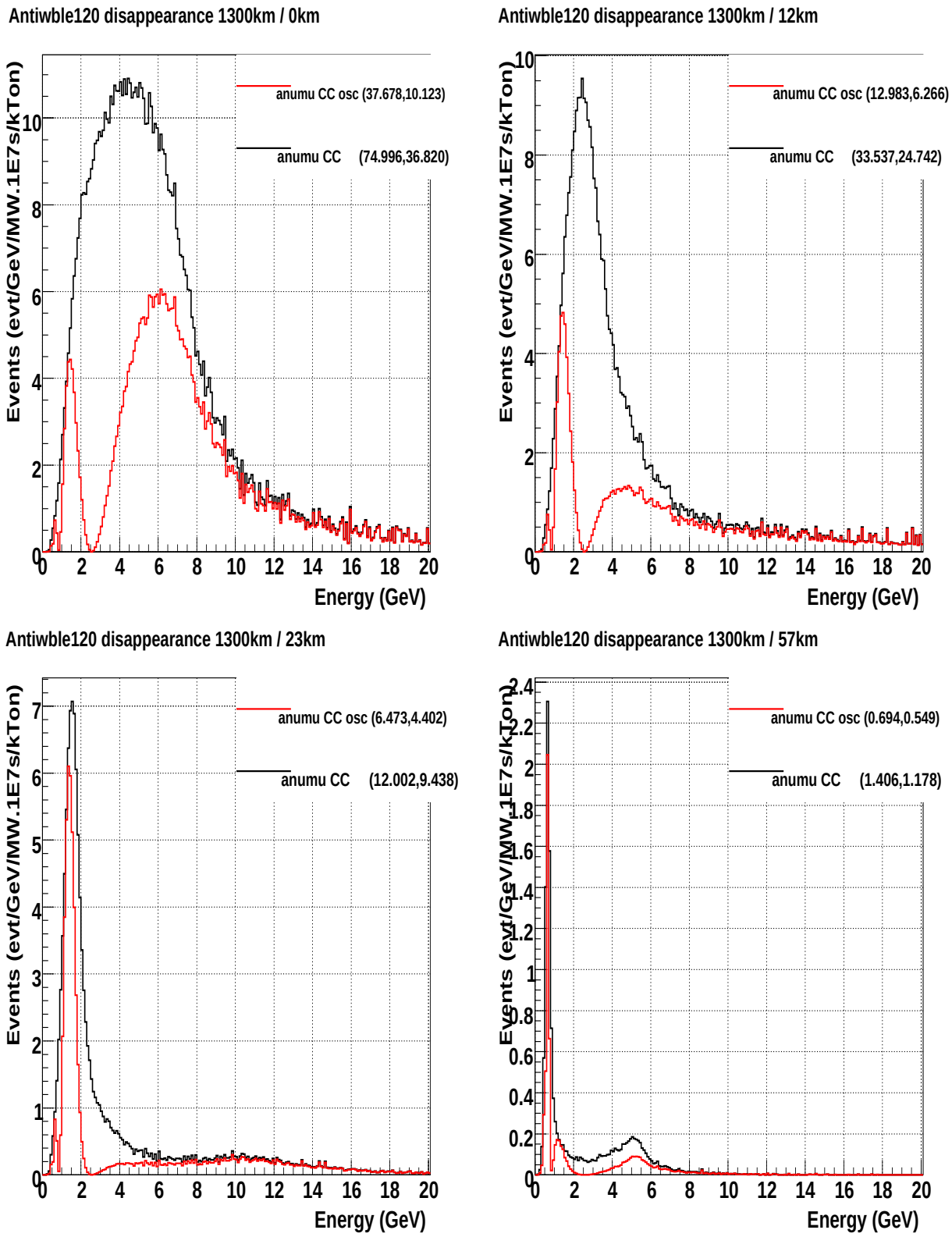

FIG. 24: $\bar{\nu}_\mu \rightarrow \bar{\nu}_\mu$ total CC interaction rates for a 120 GeV WBLE beam with various off-axis options for (0-20 GeV, 0-5GeV).

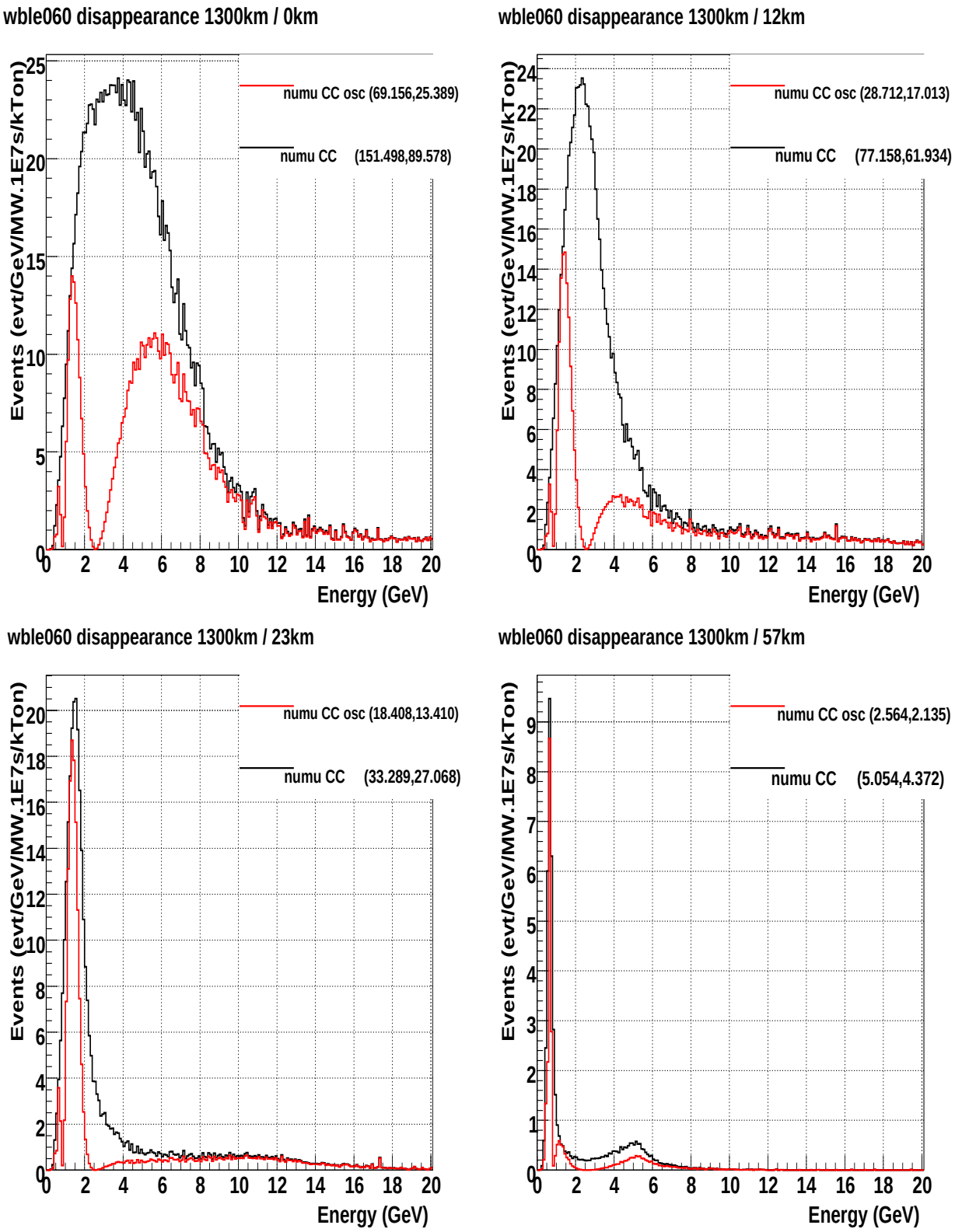

FIG. 25: $\nu_\mu \rightarrow \nu_\mu$ total CC interaction rates for a 60 GeV WBLE beam with various off-axis options for (0-20 GeV, 0-5GeV).

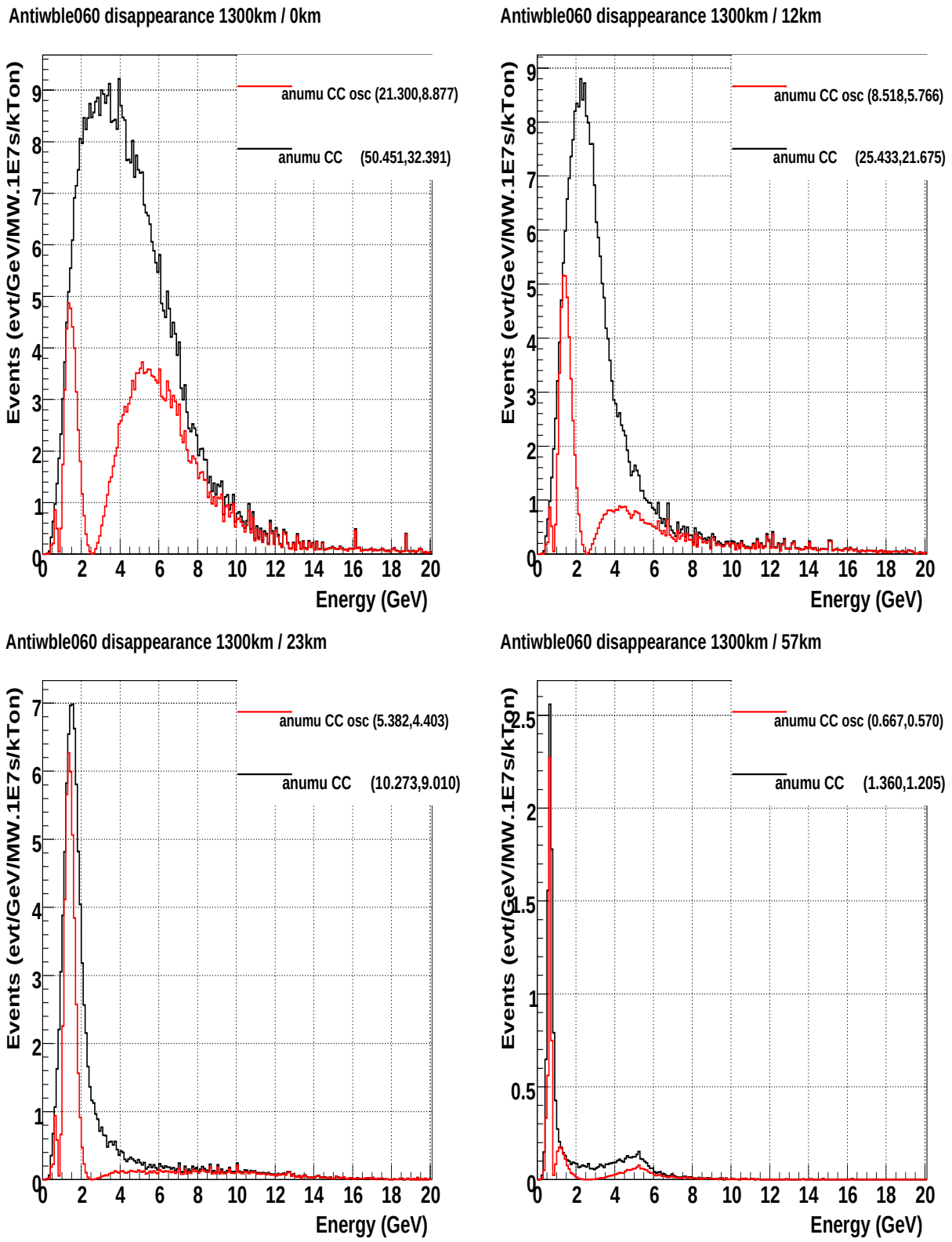

FIG. 26: $\bar{\nu}_\mu \rightarrow \bar{\nu}_\mu$ total CC interaction rates for a 60 GeV WBLE beam with various off-axis options for (0-20 GeV, 0-5GeV).

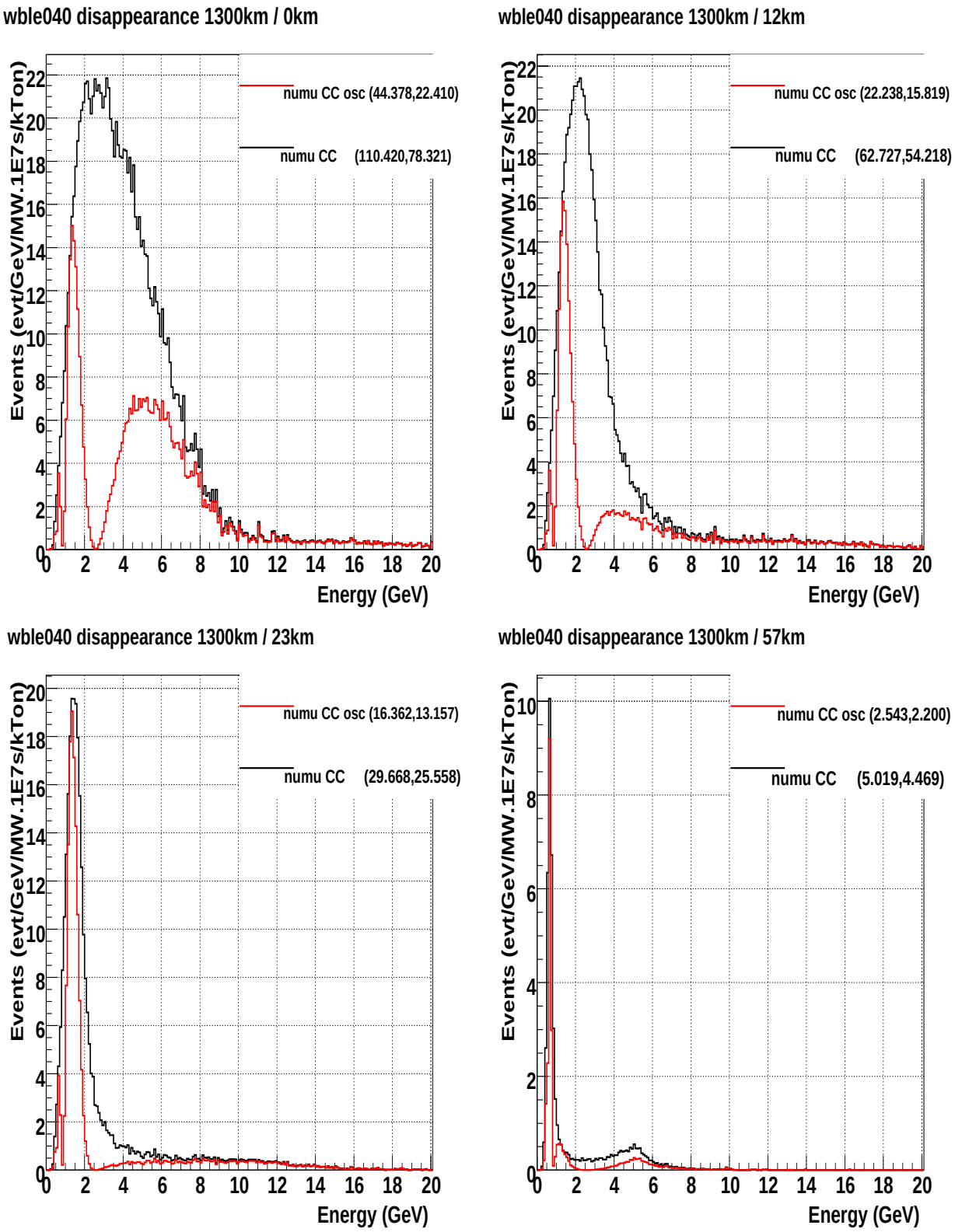

FIG. 27: $\nu_\mu \rightarrow \nu_\mu$ total CC interaction rates for a 40 GeV WBLE beam with various off-axis options for (0-20 GeV, 0-5GeV).

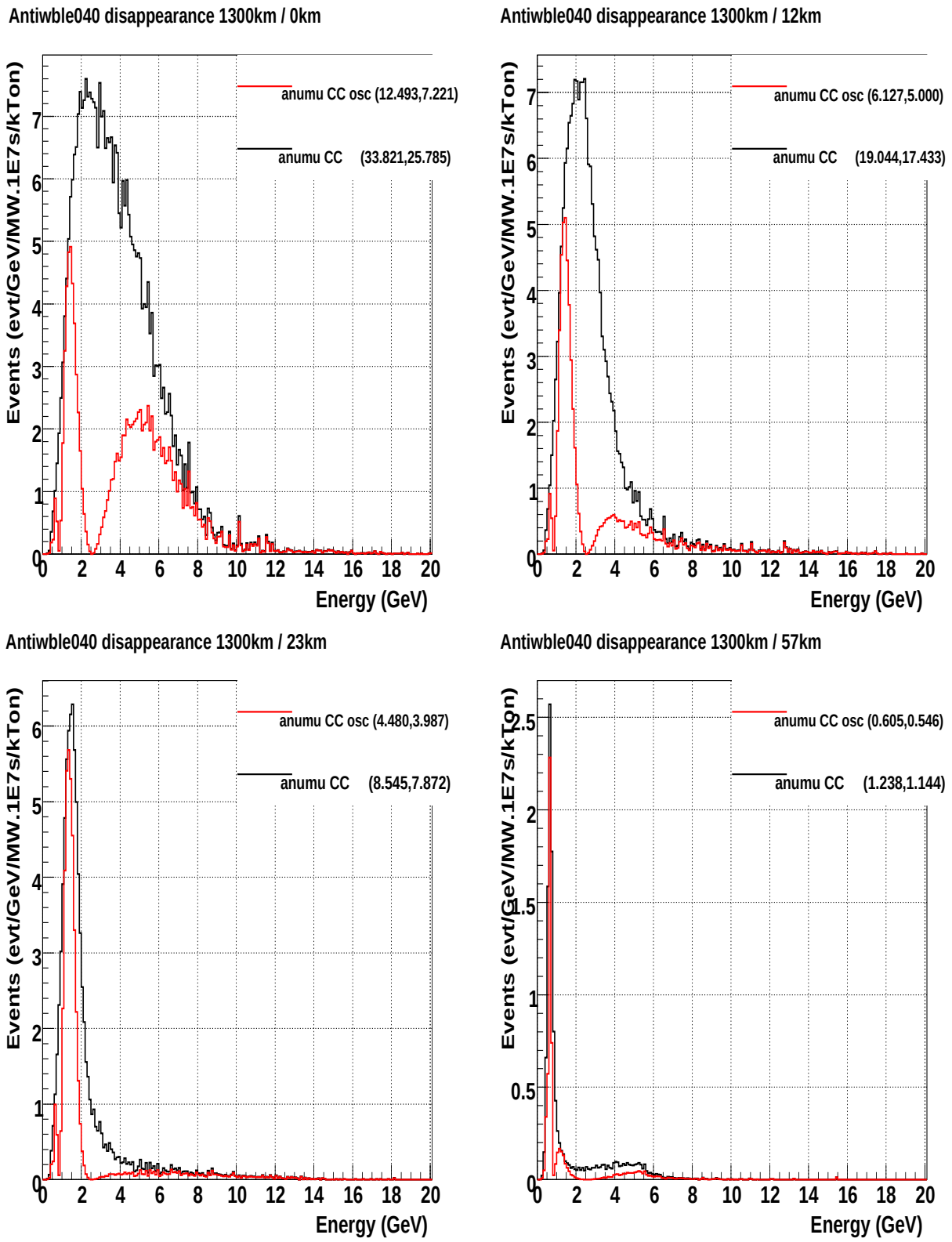

FIG. 28: $\bar{\nu}_\mu \rightarrow \bar{\nu}_\mu$ total CC interaction rates for a 40 GeV WBLE beam with various off-axis options for (0-20 GeV, 0-5GeV).

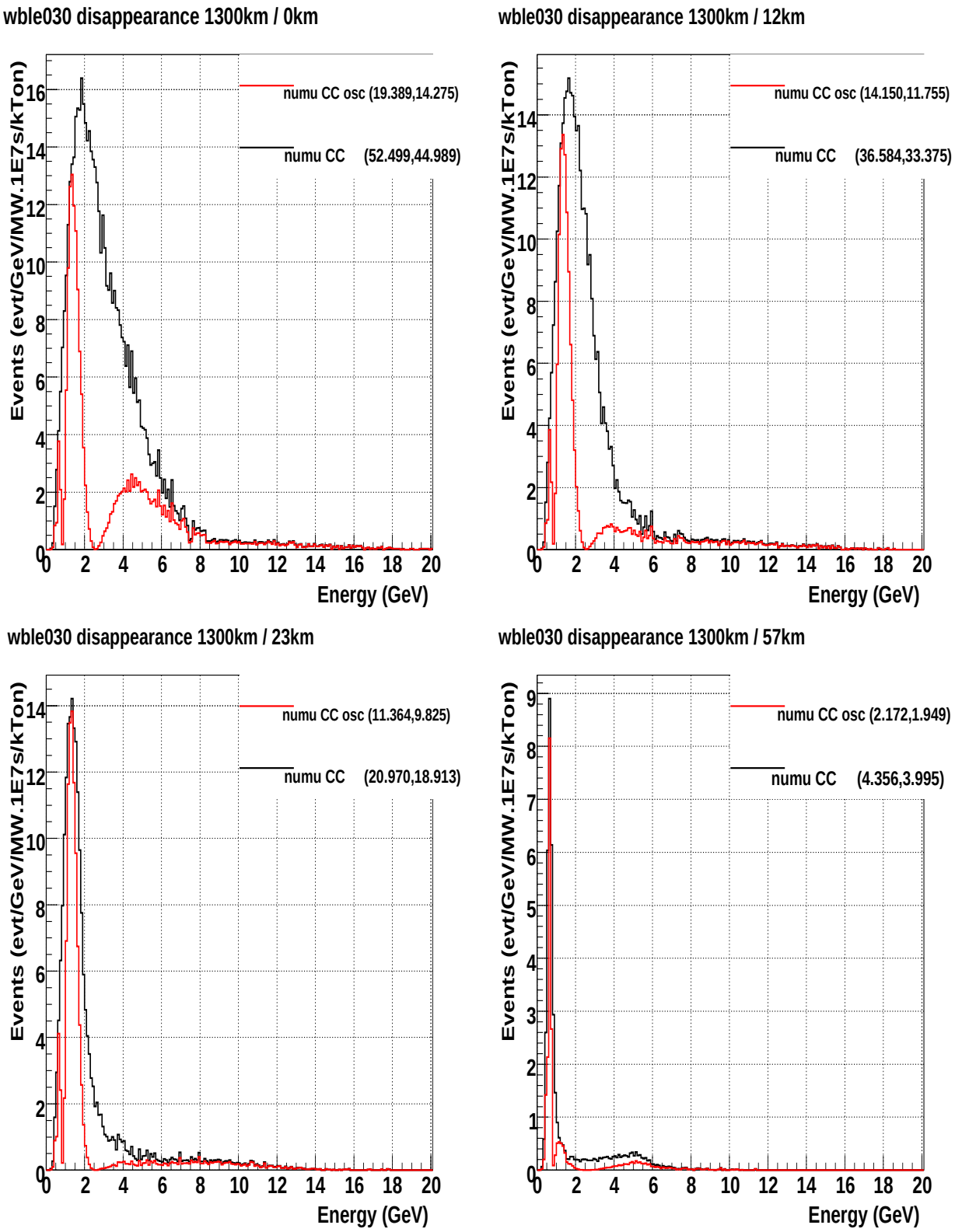

FIG. 29: $\nu_\mu \rightarrow \nu_\mu$ total CC interaction rates for a 30 GeV WBLE beam with various off-axis options for (0-20 GeV, 0-5GeV).

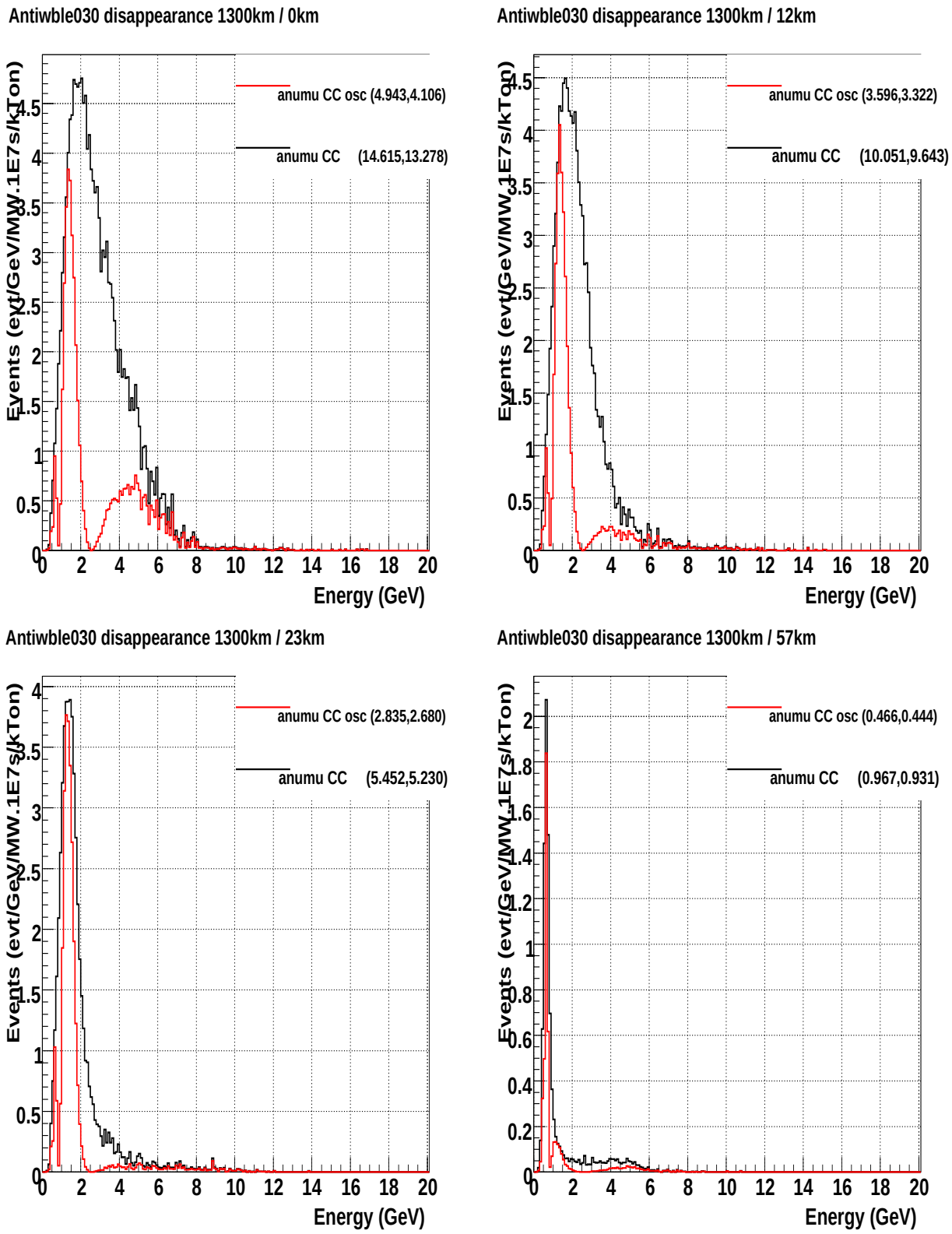

FIG. 30: $\bar{\nu}_\mu \rightarrow \bar{\nu}_\mu$ total CC interaction rates for a 30 GeV WBLE beam with various off-axis options for (0-20 GeV, 0-5GeV).

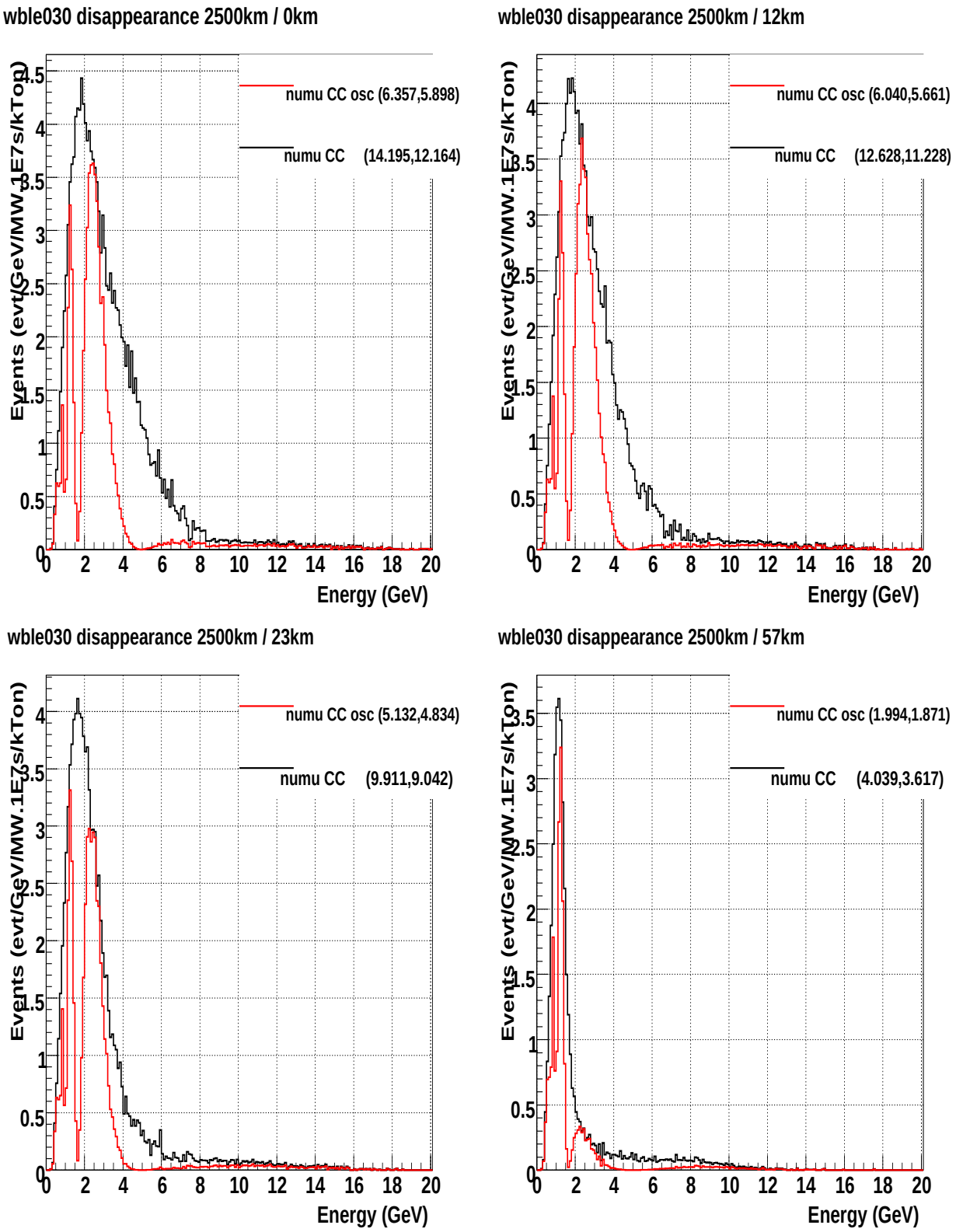

FIG. 31: $\nu_\mu \rightarrow \nu_\mu$ total CC interaction rates for a 30 GeV WBLE beam with various off-axis options for (0-20 GeV, 0-5GeV).

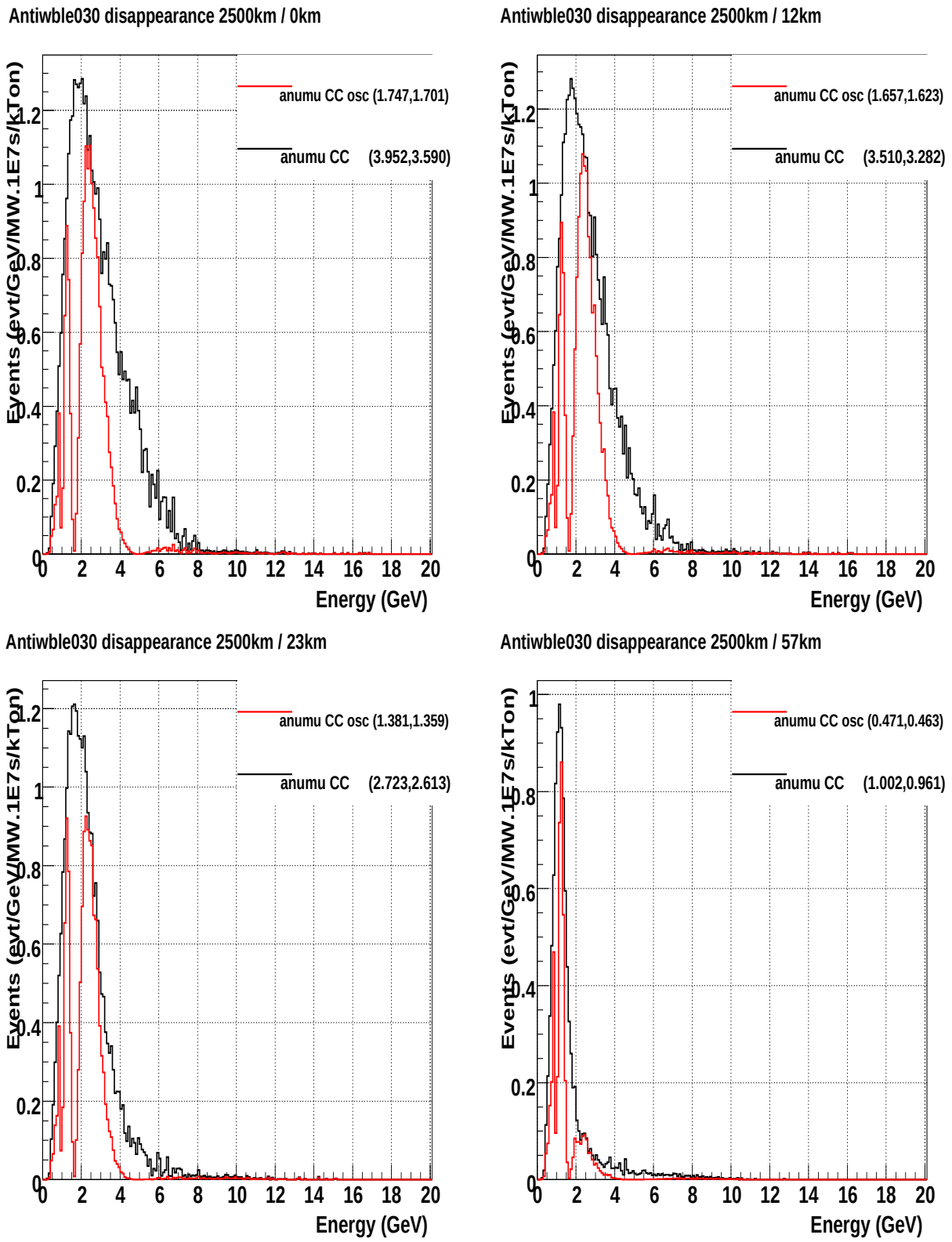

FIG. 32: $\bar{\nu}_\mu \rightarrow \bar{\nu}_\mu$ total CC interaction rates for a 30 GeV WBLE beam with various off-axis options for (0-20 GeV, 0-5GeV).

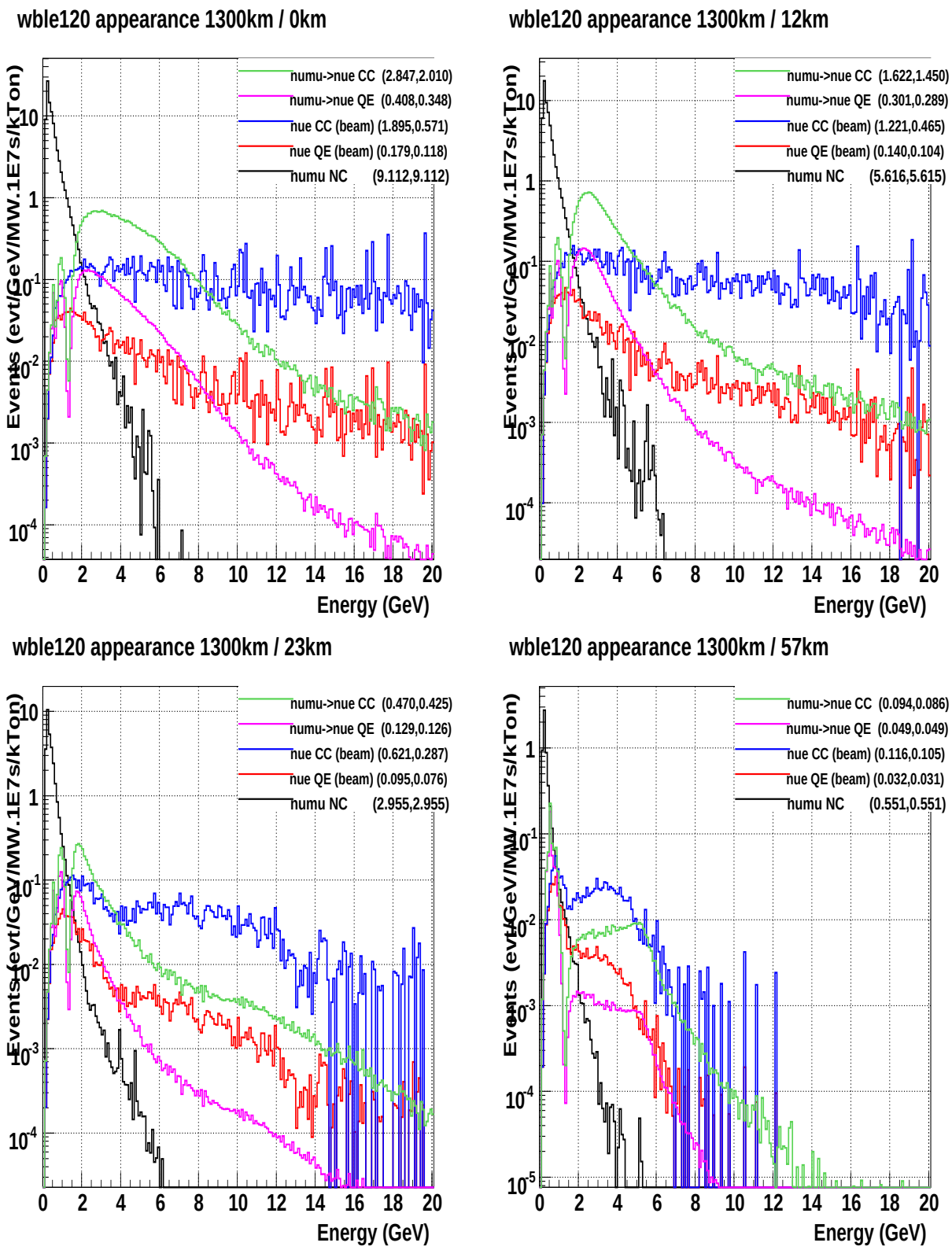

FIG. 33: $\nu_\mu \to \nu_e$ appearance rates and single π^0 background rates for a 120 GeV WBLE beam with various off-axis options for (0-20 GeV, 0-5GeV).

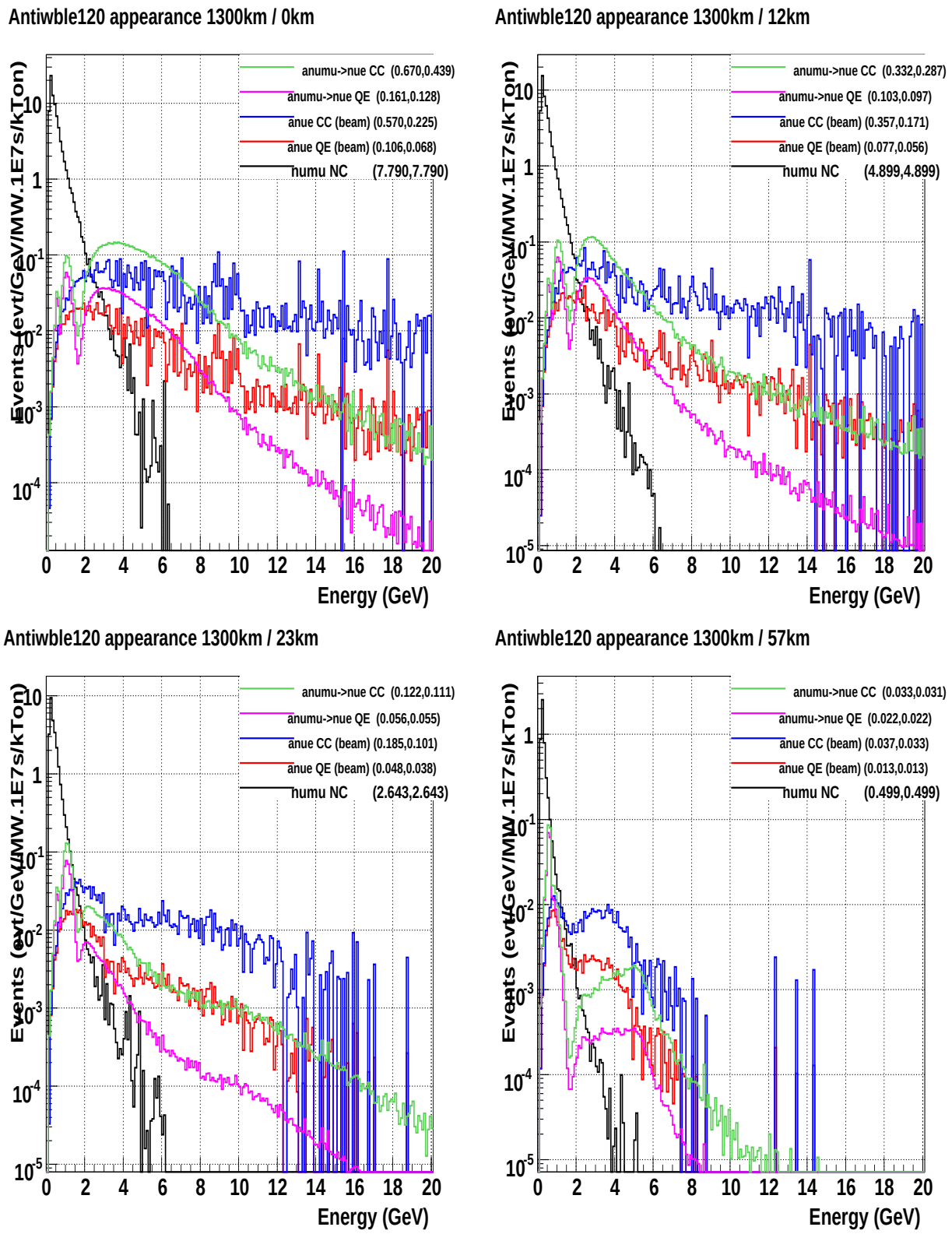

FIG. 34: $\nu_\mu \to \nu_e$ appearance rates and single π^0 background rates for a 120 GeV WBLE beam with various off-axis options for (0-20 GeV, 0-5GeV).

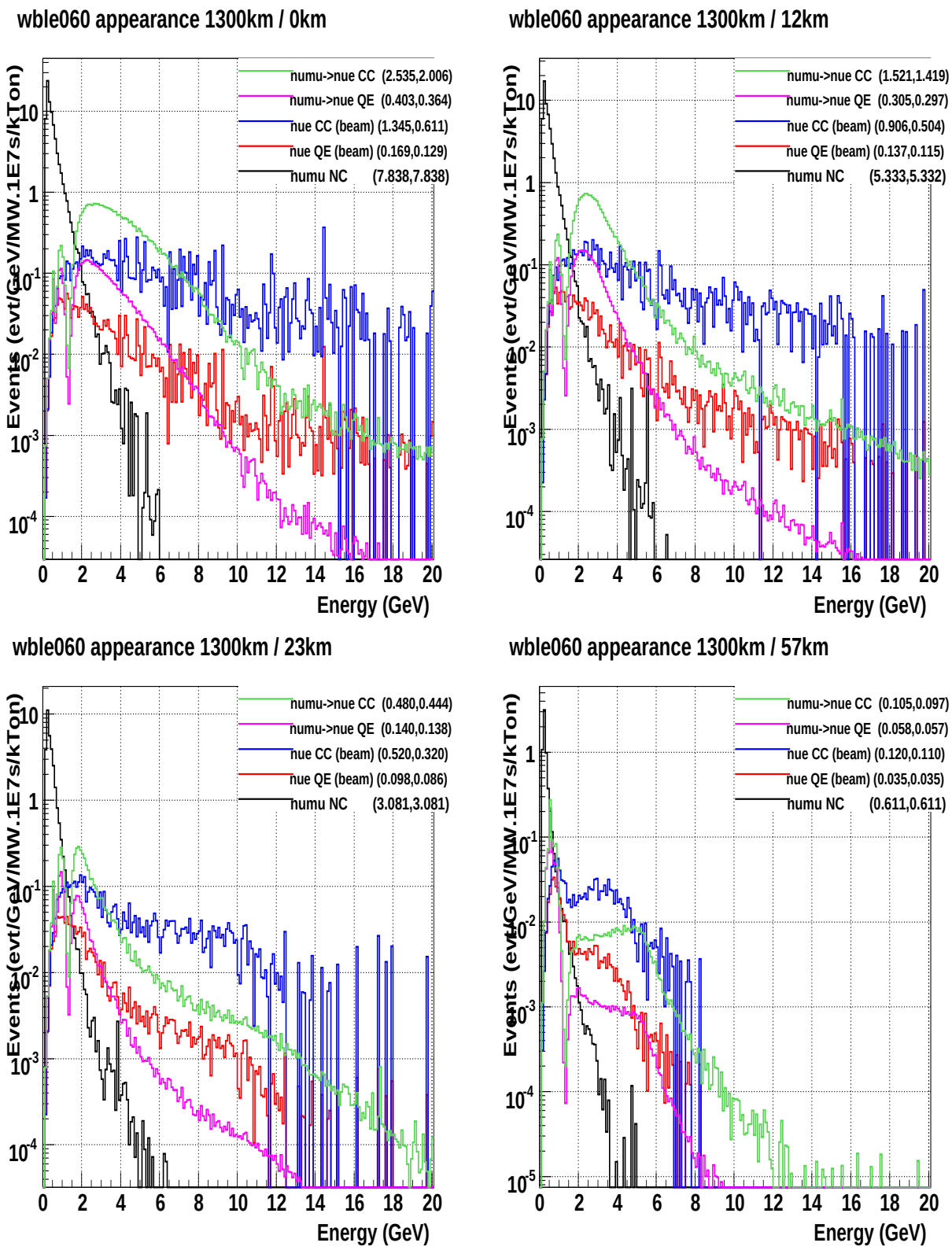

FIG. 35: $\nu_\mu \rightarrow \nu_e$ appearance rates and single π^0 background rates for a 60 GeV WBLE beam with various off-axis options for (0-20 GeV, 0-5GeV).

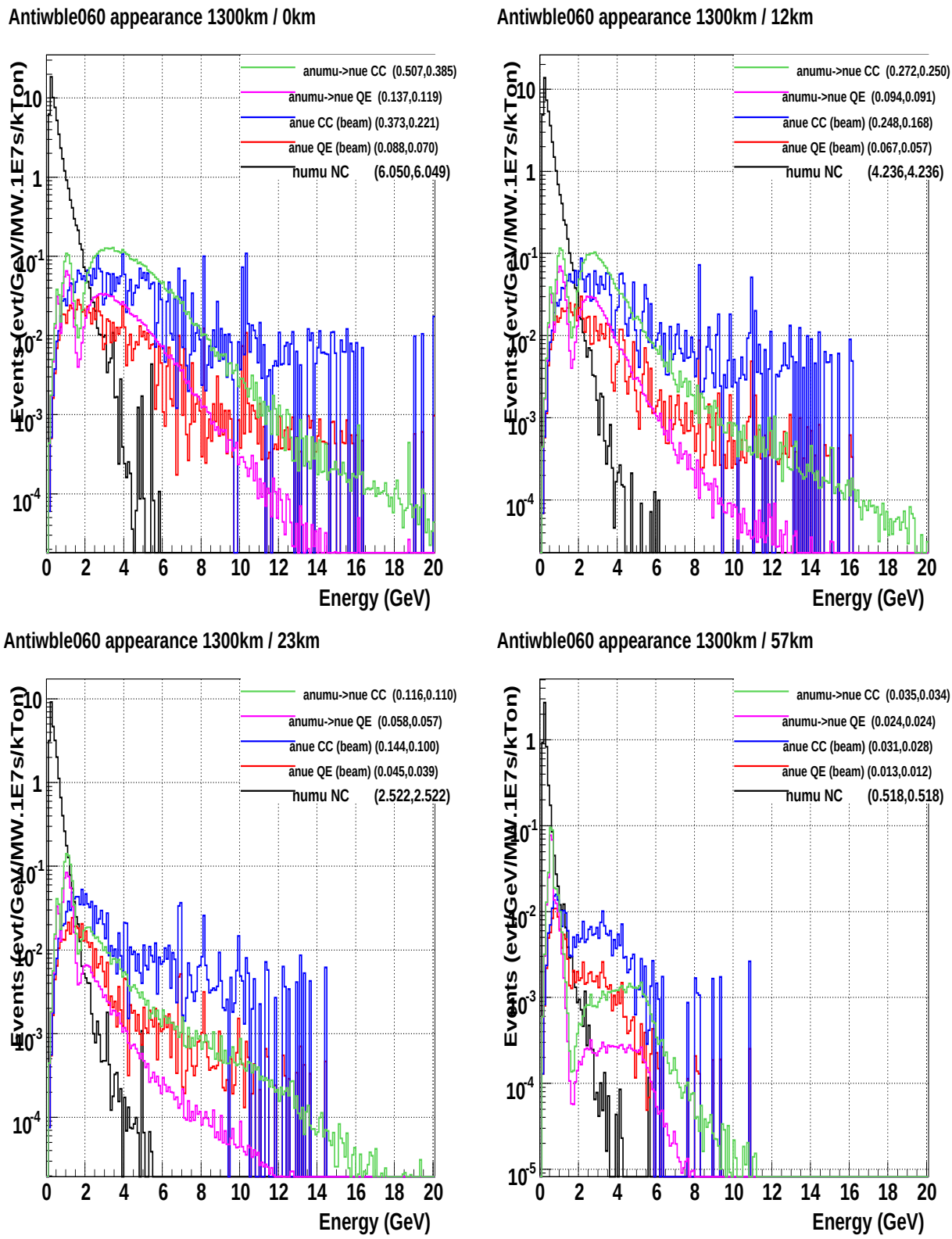

FIG. 36: $\nu_\mu \rightarrow \nu_e$ appearance rates and single π^0 background rates for a 60 GeV WBLE beam with various off-axis options for (0-20 GeV, 0-5GeV).

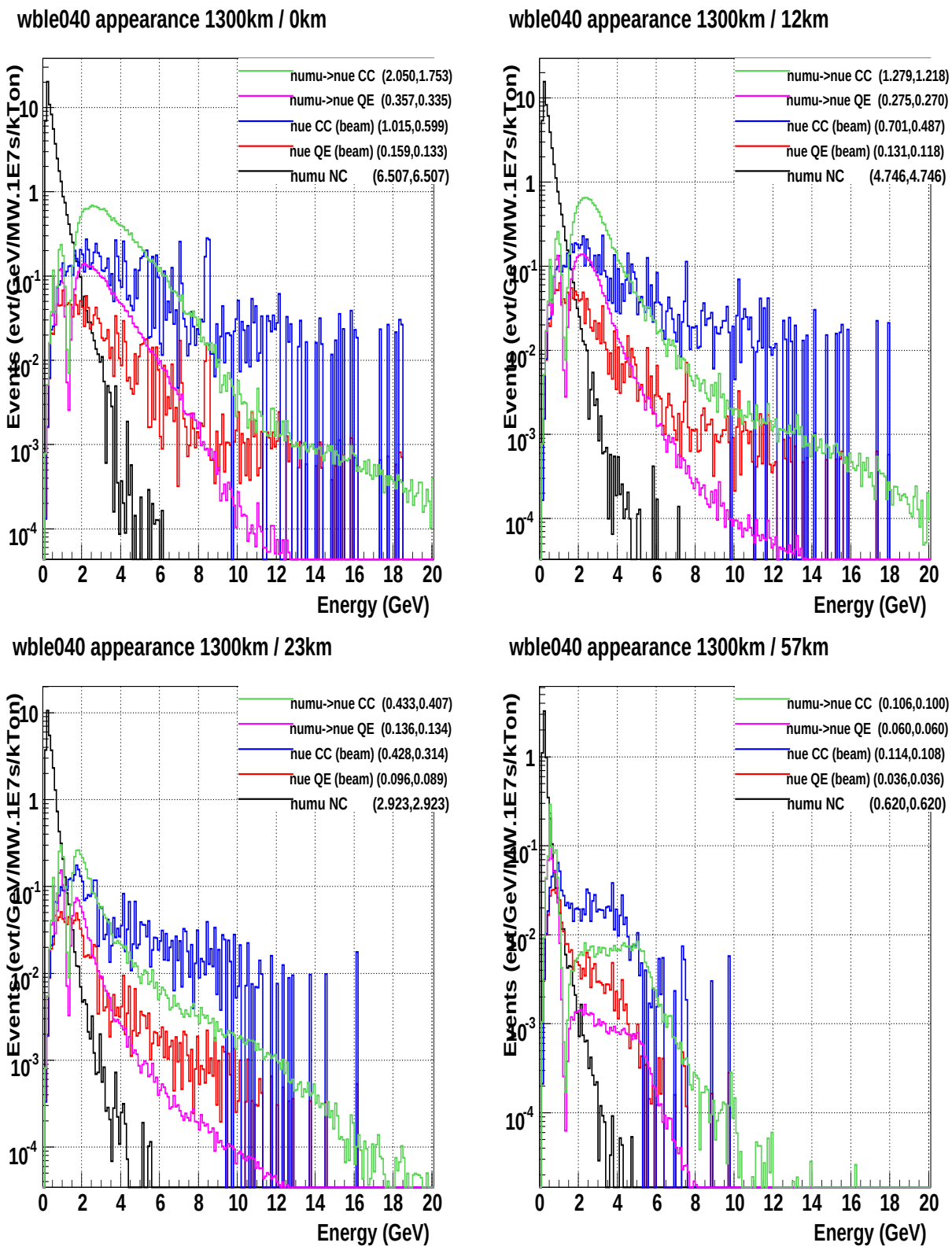

FIG. 37: $\nu_\mu \rightarrow \nu_e$ appearance rates and single π^0 background rates for a 40 GeV WBLE beam with various off-axis options for (0-20 GeV, 0-5GeV).

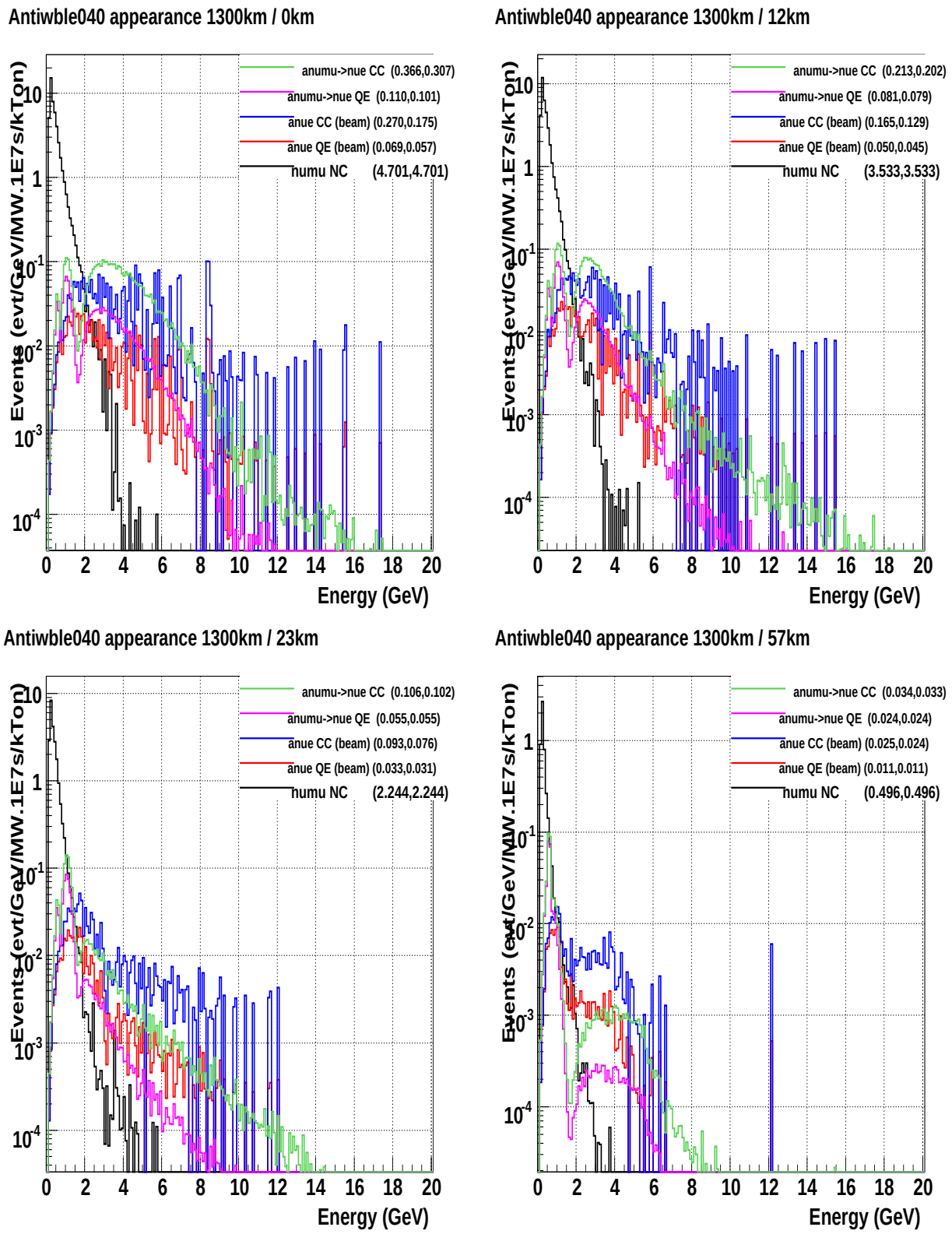

FIG. 38: $\nu_\mu \rightarrow \nu_e$ appearance rates and single π^0 background rates for a 40 GeV WBLE beam with various off-axis options for (0-20 GeV, 0-5GeV).

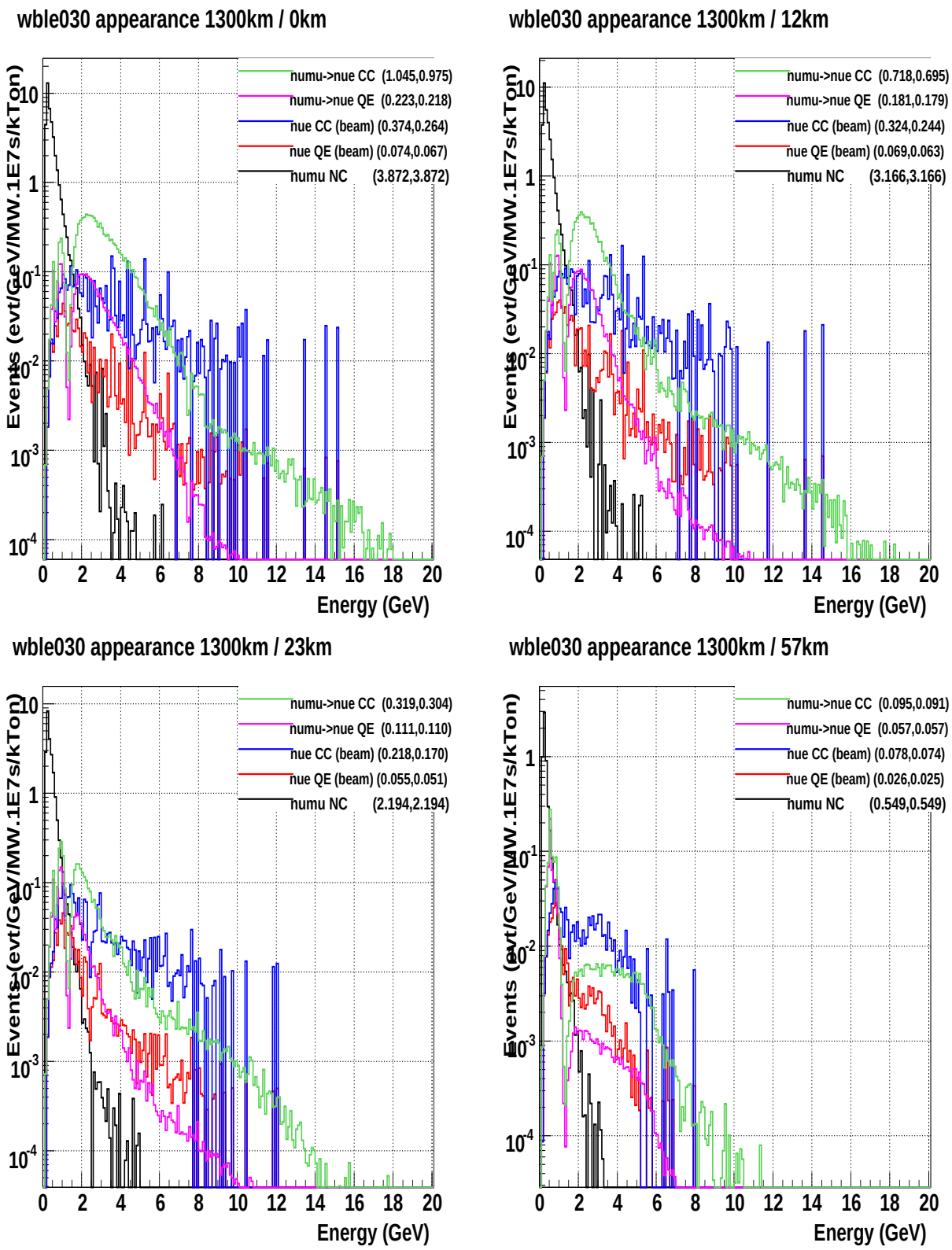

FIG. 39: $\nu_\mu \rightarrow \nu_e$ appearance rates and single π^0 background rates for a 30 GeV WBLE beam with various off-axis options for (0-20 GeV, 0-5GeV).

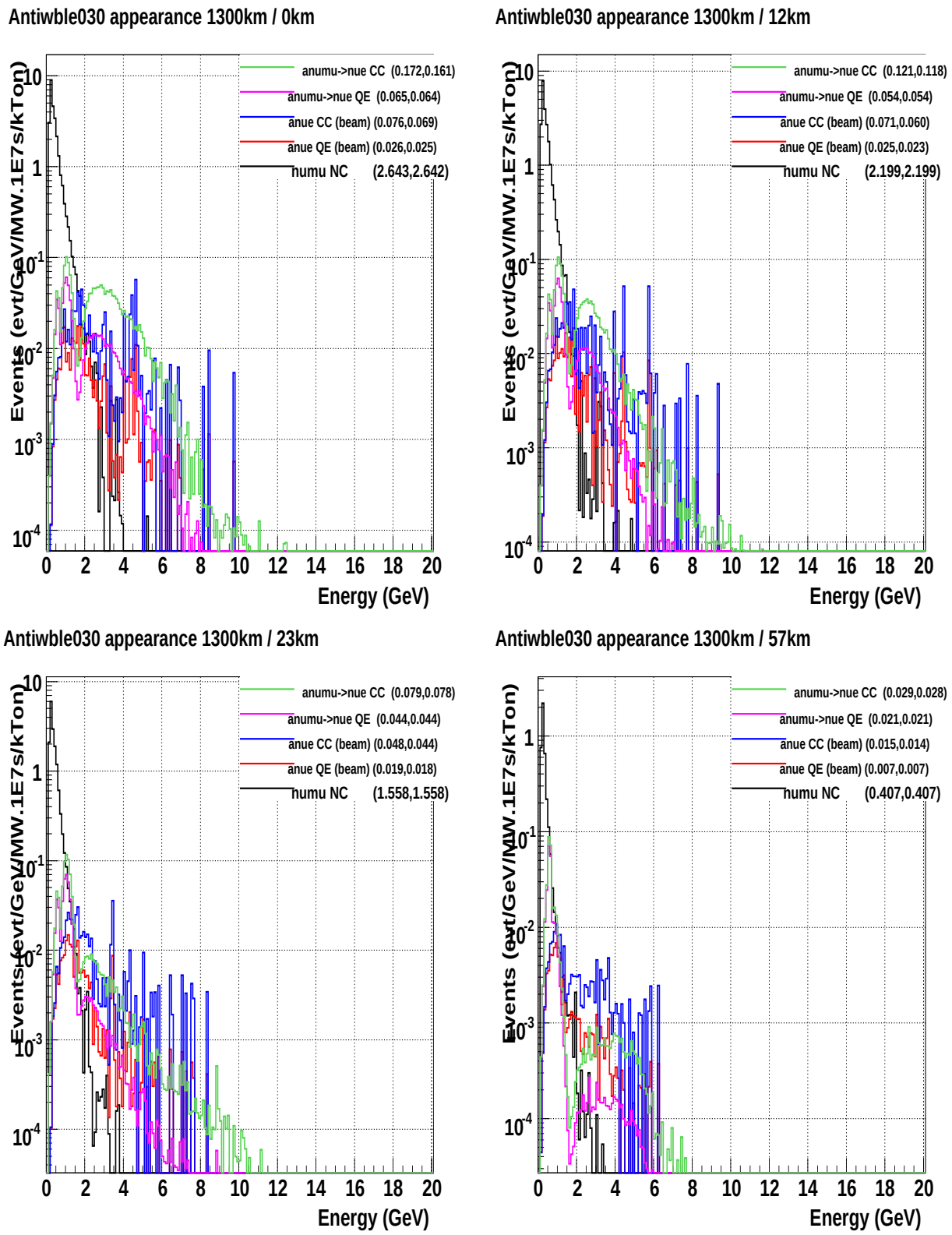

FIG. 40: $\nu_\mu \rightarrow \nu_e$ appearance rates and single π^0 background rates for a 30 GeV WBLE beam with various off-axis options for (0-20 GeV, 0-5GeV).

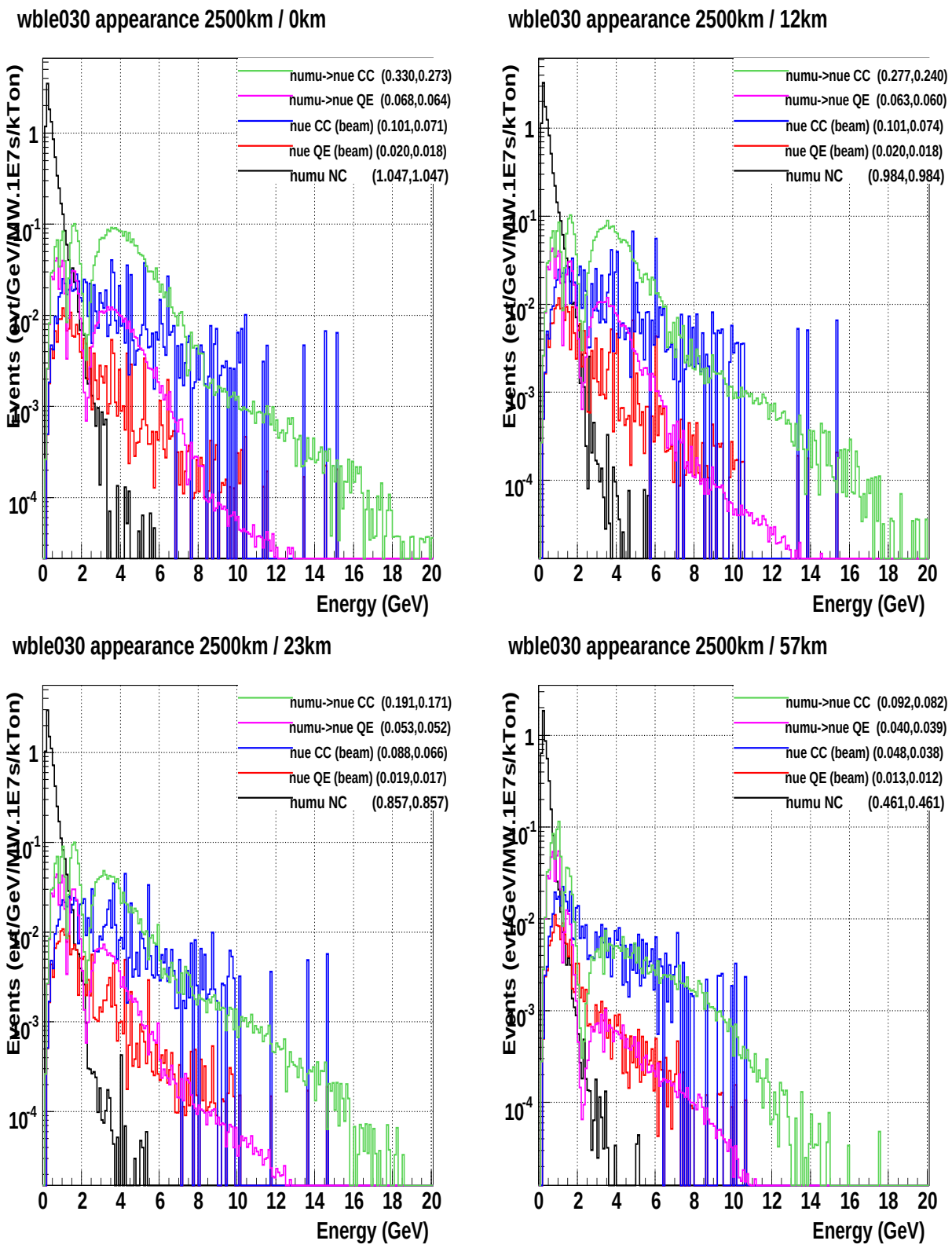

FIG. 41: $\nu_\mu \rightarrow \nu_e$ appearance rates and single π^0 background rates for a 30 GeV WBLE beam with various off-axis options for (0-20 GeV, 0-5GeV).

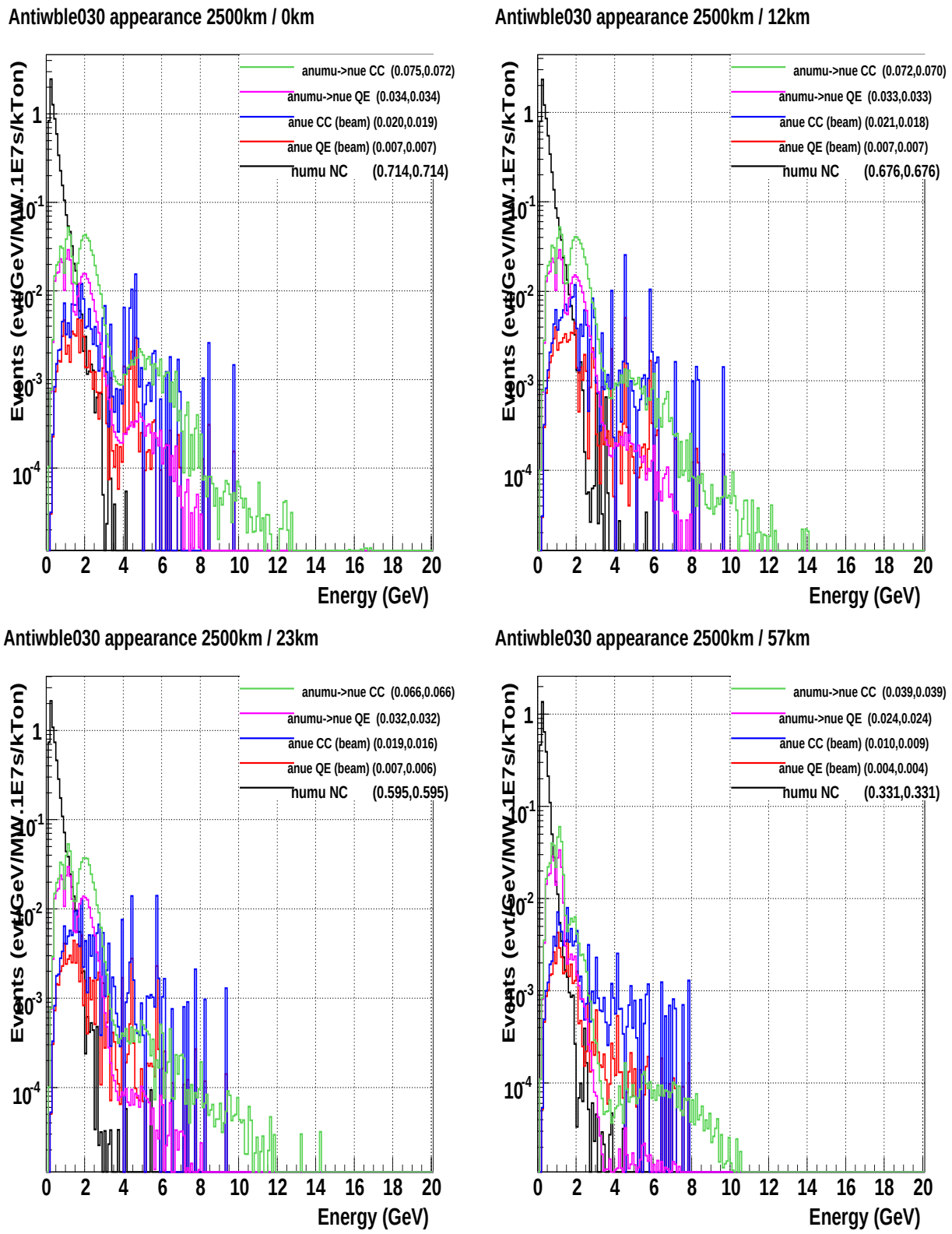

FIG. 42: $\nu_\mu \rightarrow \nu_e$ appearance rates and single π^0 background rates for a 30 GeV WBLE beam with various off-axis options for (0-20 GeV, 0-5GeV).